Supporting Information

Flowing Scalable Production of Sulfenamides by Active Sites Tuned Lacunary Polyoxometalate Foams

Gang Liu,[a,†] Yuquan Qi,[a,†] Yifa Chen,*[,b] Jiashuai Li,[a] Yilan Chen,[a] Zhen Li,[a] Guodong Shen,[a] Delong Ma,[a,c] Yunfeng Li[a,c] and Xianqiang Huang*[,a]

[a] *Shandong Provincial Key Laboratory of Chemical Energy Storage and Novel Cell Technology, School of Chemistry & Chemical Engineering, Liaocheng University, Liaocheng, 252059, Shandong, P. R. China.*

[b] *School of Chemistry, South China Normal University, Guangzhou, 510006, P. R. China.*

[c] *National Rubber Additive Engineering Technology Center, Liaocheng, Shandong 252059, China.*

** Corresponding Author: X. Huang (hxq@lcu.edu.cn); Y. Chen (chyf927821@163.com).*

[†] *These authors contributed equally to this work.*

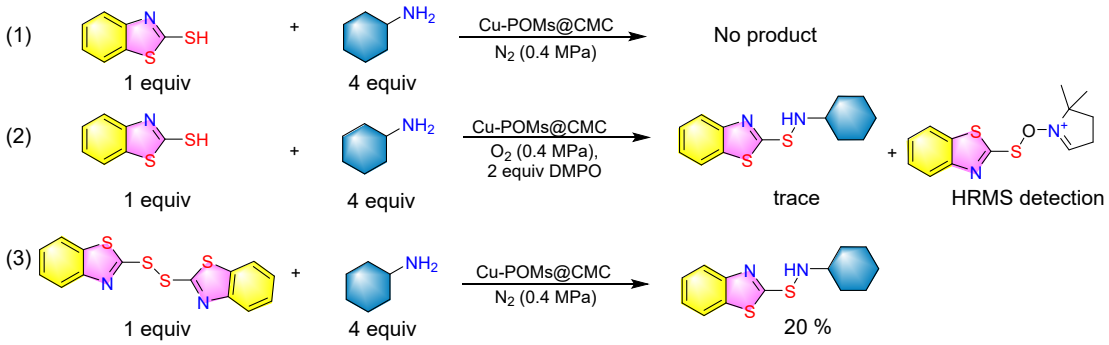

Scheme S1. General procedure for the control experiments.

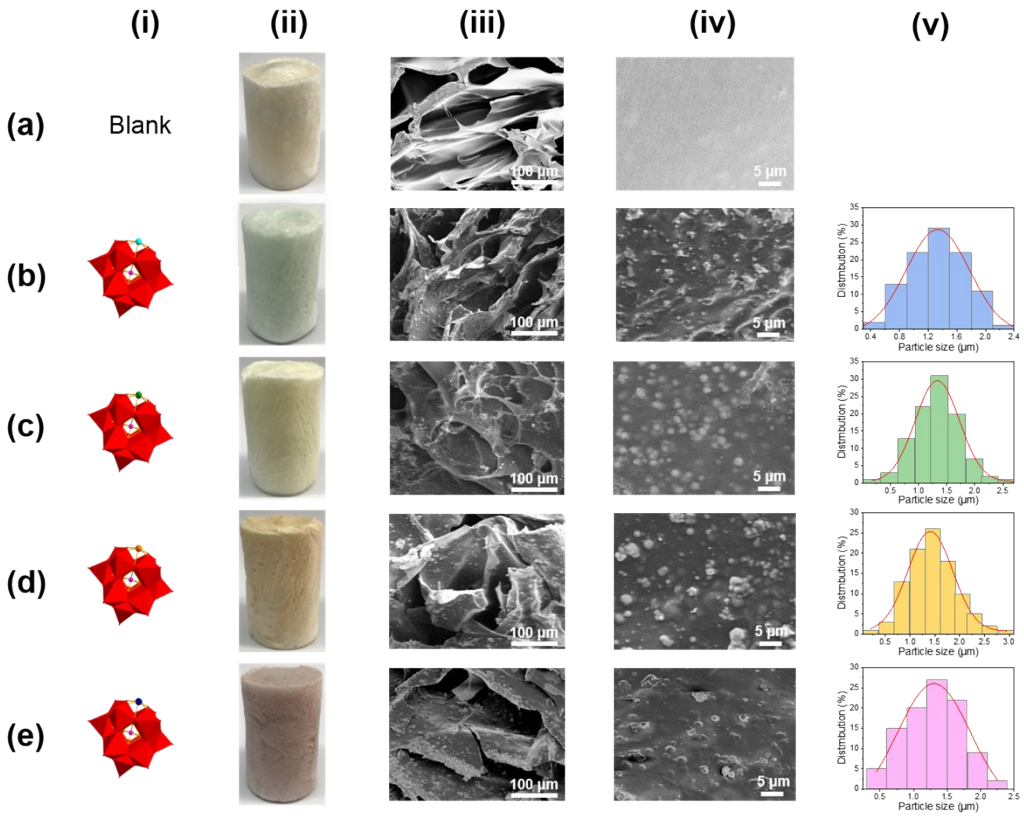

Figure S1. SEM characterization of four L-POMs@Foam. (a) CMC foam. (b) Cu-LPOMs@CMC (29 wt%). (c) Ni-LPOMs@CMC (29 wt%). (d) Mn-LPOMs@CMC (29 wt%). (e) Co-LPOMs@CMC (29 wt%). (i) Lacunary polyoxometalates. (ii) Photo images, (iii, iv) SEM images, (v) Size-distribution histograms of the prepared foams.

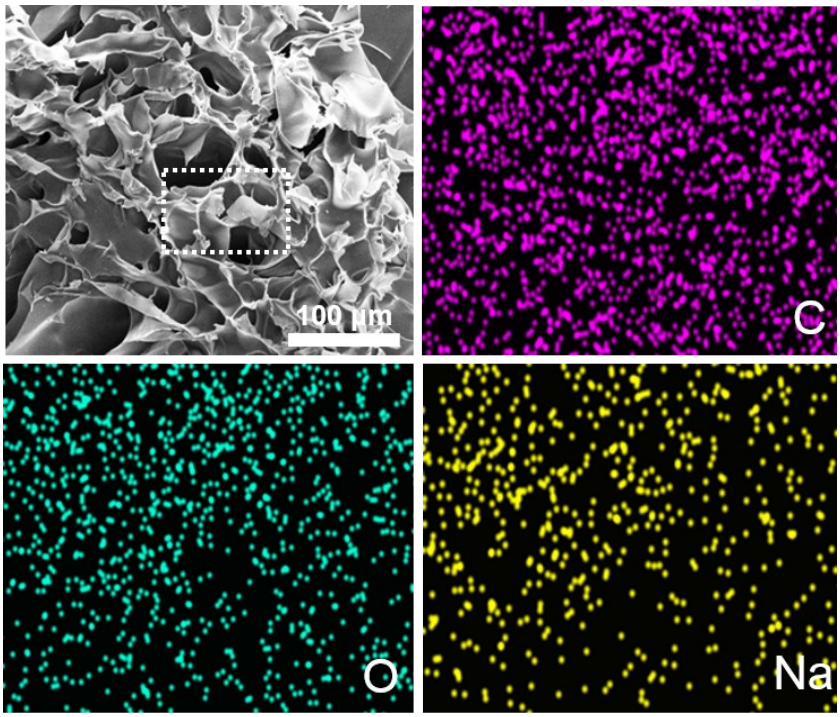

Figure S2. Elemental mapping of CMC foam.

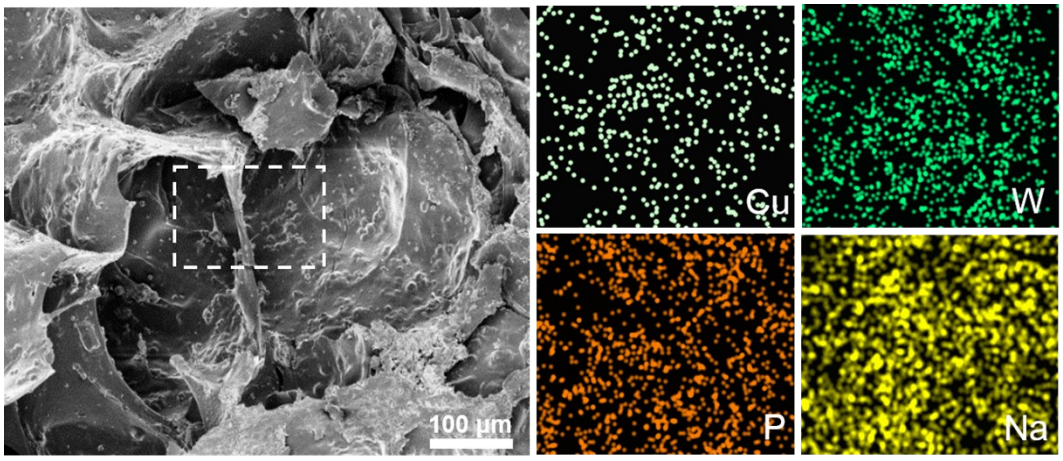

Figure S3. Elemental mapping of Cu-LPOMs@CMC (29 wt%).

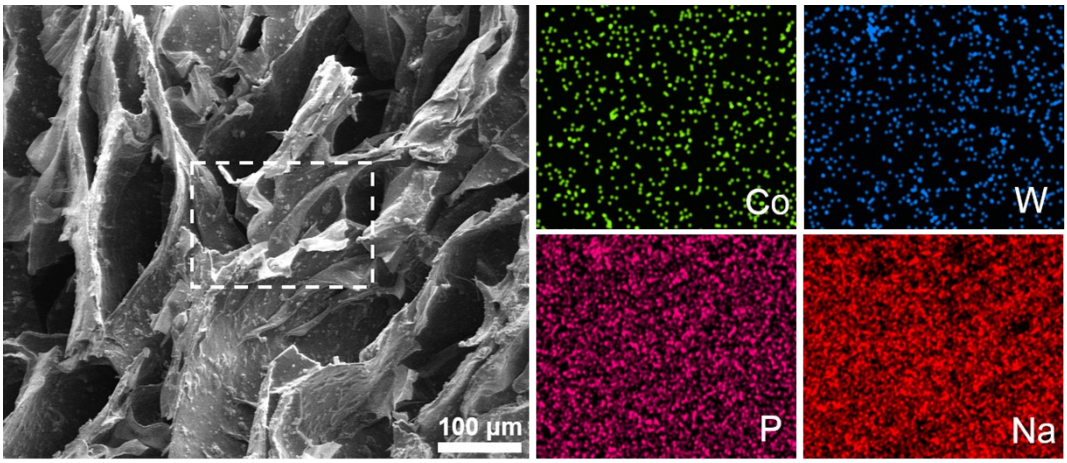

Figure S4. Elemental mapping of Co-LPOMs@CMC (29 wt%).

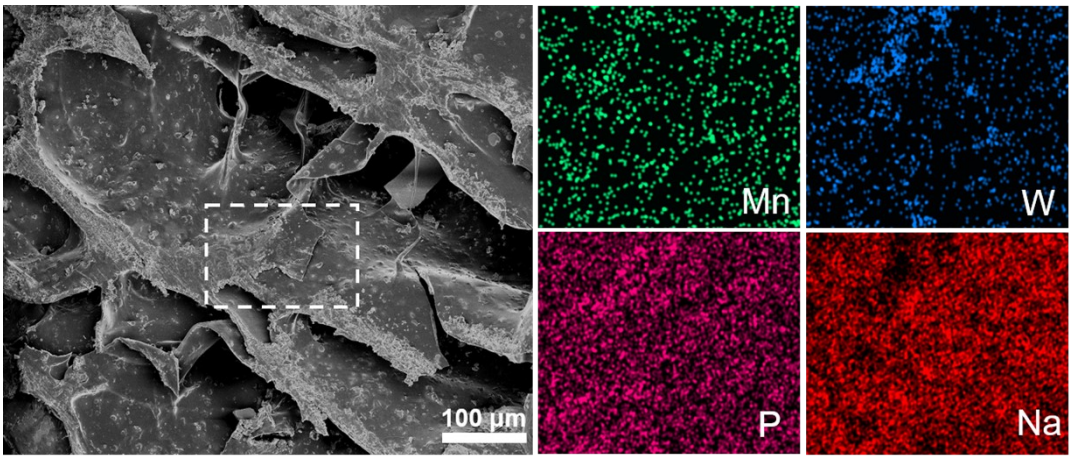

Figure S5. Elemental mapping of Mn-LPOMs@CMC (29 wt%).

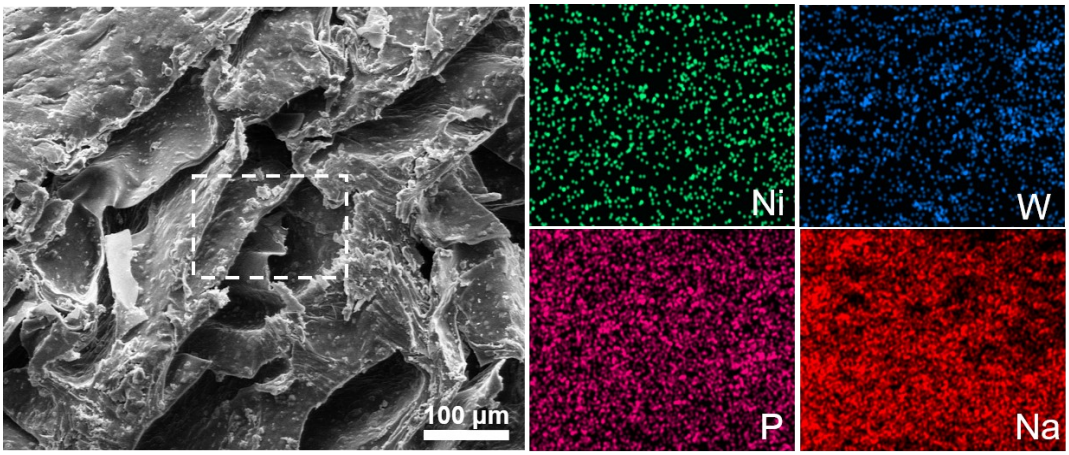

Figure S6. Elemental mapping of Ni-LPOMs@CMC (29 wt%).

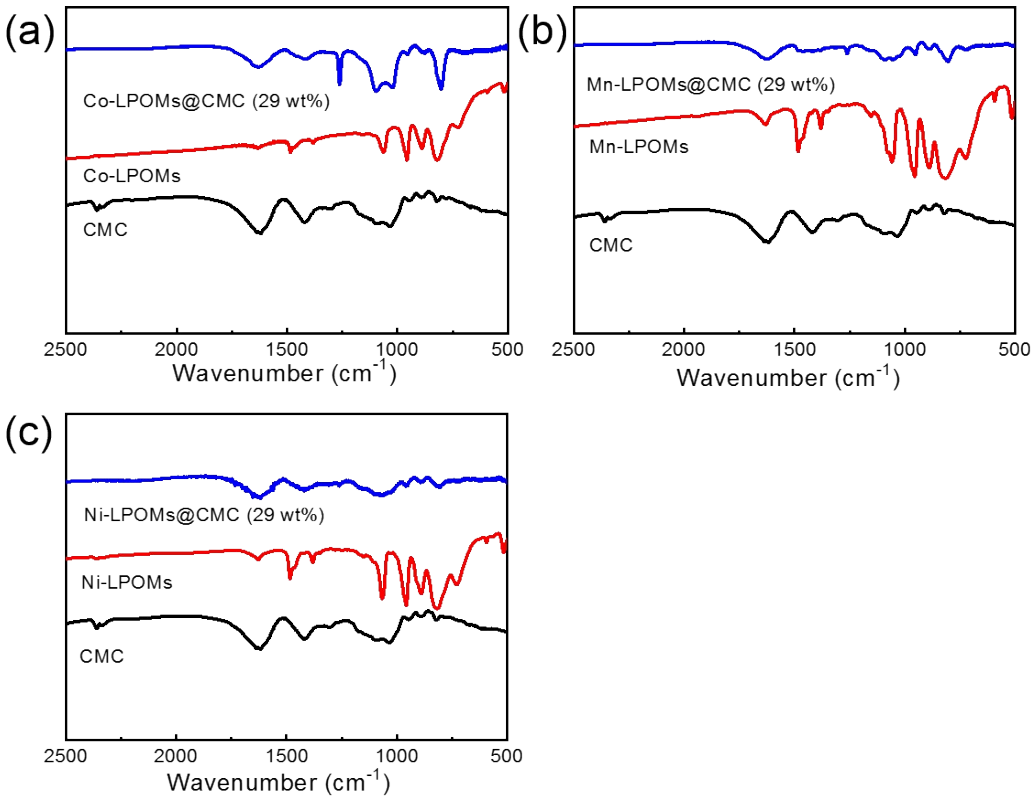

Figure S7. FT-IR spectra of TM-LPOMs@CMC (TM = Co, Mn and Ni). (a) FT-IR spectra of CMC, Co-LPOMs and Co-LPOMs@CMC (29 wt%). (b) FT-IR spectra of CMC, Mn-LPOMs and Mn-LPOMs@CMC (29 wt%). (c) FT-IR spectra of CMC, Ni-LPOMs and Ni-LPOMs@CMC (29 wt%).

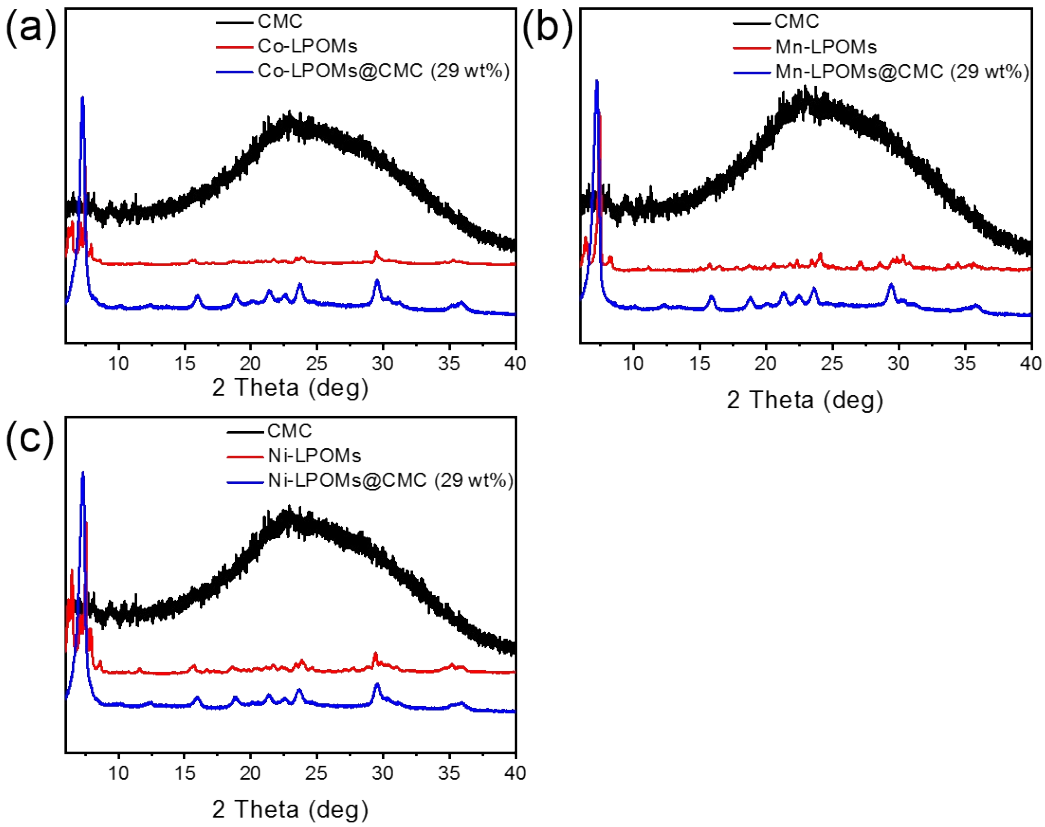

Figure S8. PXRD patterns of TM-LPOMs@CMC (TM = Co, Mn and Ni). (a) PXRD patterns of CMC, Co-LPOMs and Co-LPOMs@CMC (29 wt%). (b) PXRD patterns of CMC, Mn-LPOMs and Mn-LPOMs@CMC (29 wt%). (c) PXRD patterns of CMC, Ni-LPOMs and Ni-LPOMs@CMC (29 wt%).

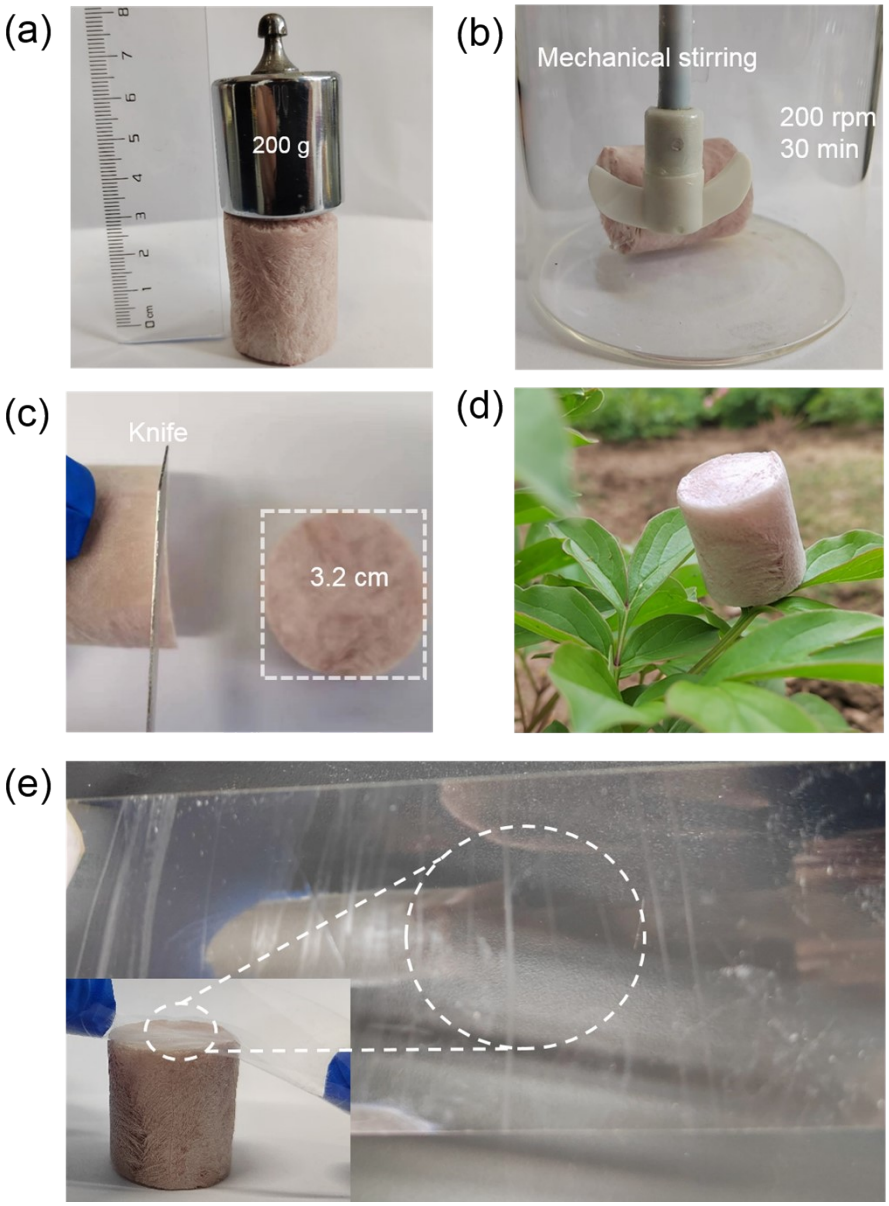

Figure S9. Physical properties of Co-LPOMs@CMC (29 wt%). (a) The photo image of the pressing experiment. (b) Mechanical stability test of the foam. (c) The photo image of using a knife to cut the foam into a fixed shape. (d) The photograph of the foam material standing on a leaf. (e) The photo image of the foam after the scotch tape stick-and-peel test.

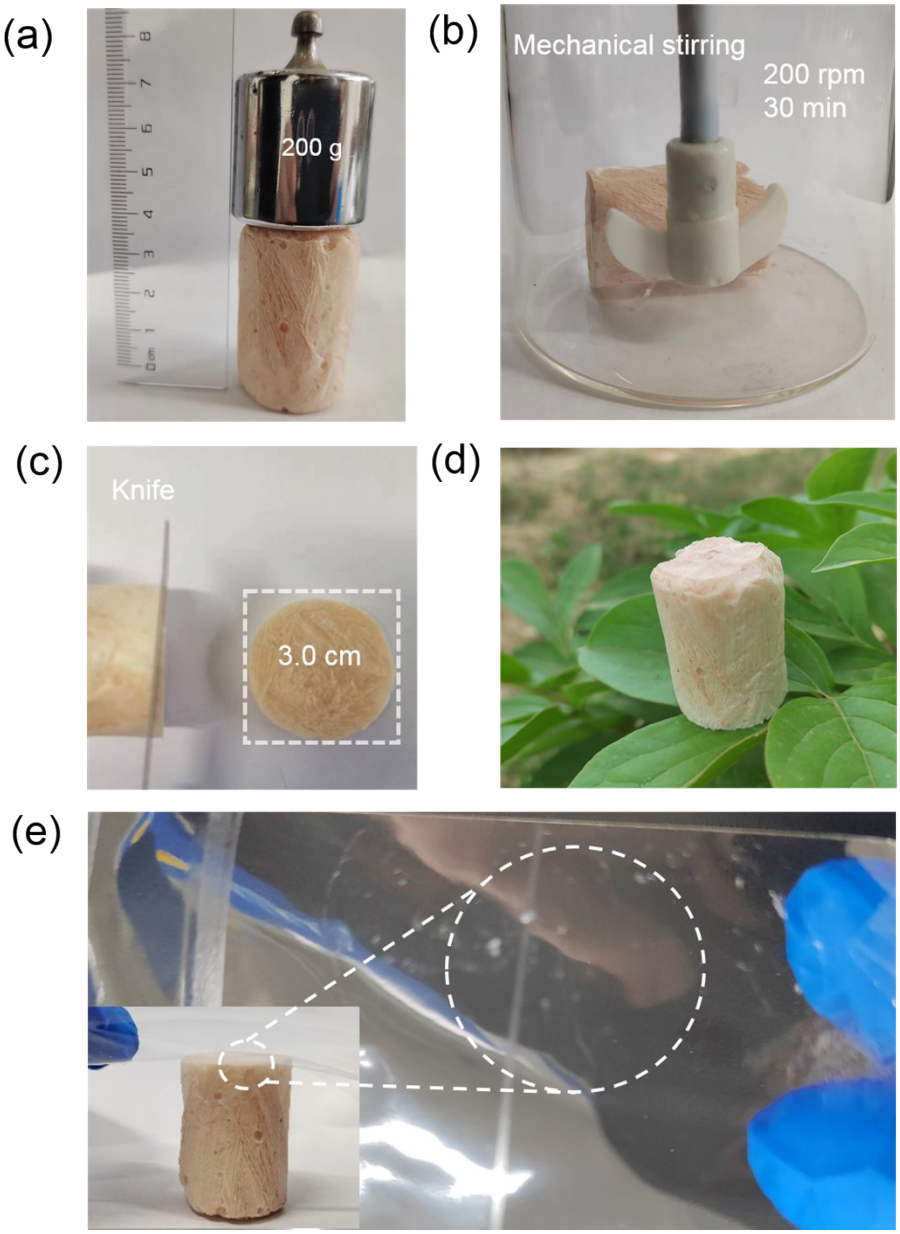

Figure S10. Physical properties of Mn-LPOMs@CMC (29 wt%). (a) The photo image of the pressing experiment. (b) Mechanical stability test of the foam. (c) The photo image of using a knife to cut the foam into a fixed shape. (d) The photograph of the foam material standing on a leaf. (e) The photo image of the foam after the scotch tape stick-and-peel test.

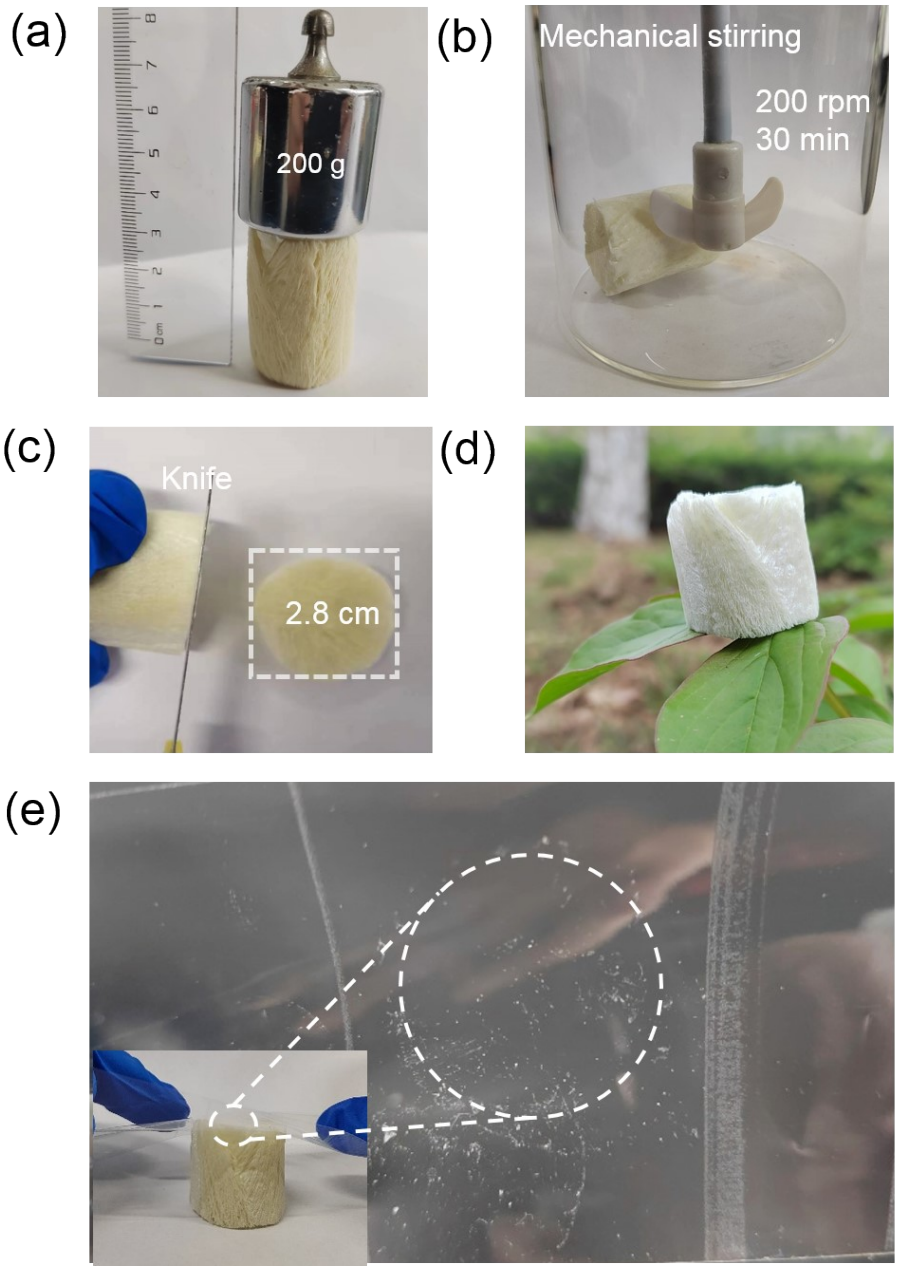

Figure S11. Physical properties of Ni-LPOMs@CMC (29 wt%). (a) The photo image of the pressing experiment. (b) Mechanical stability test of the foam. (c) The photo image of using a knife to cut the foam into a fixed shape. (d) The photograph of the foam material standing on a leaf. (e) The photo image of the foam after the scotch tape stick-and-peel test.

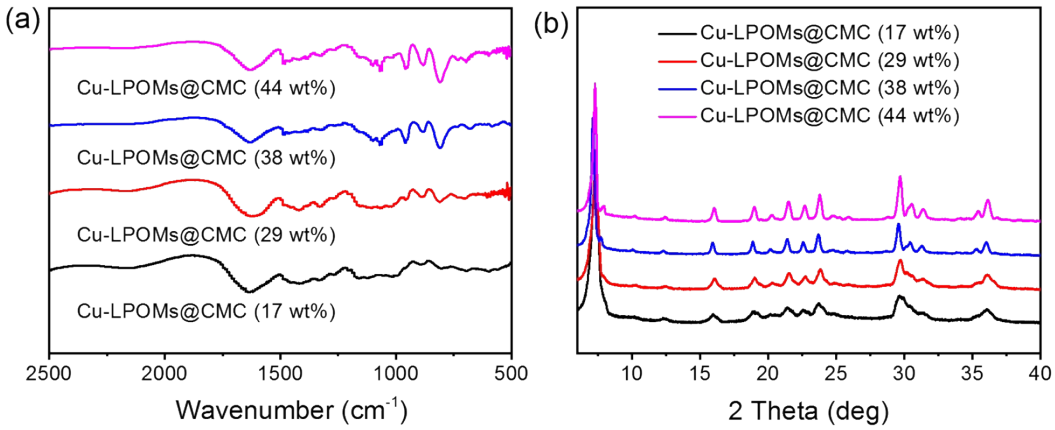

Figure S12. FT-IR and PXRD of the Cu-LPOMs@CMC foams with various Cu-LPOMs loadings. (a) FT-IR spectrum of Cu-LPOMs@CMC. (b) PXRD patterns of Cu-LPOMs@CMC.

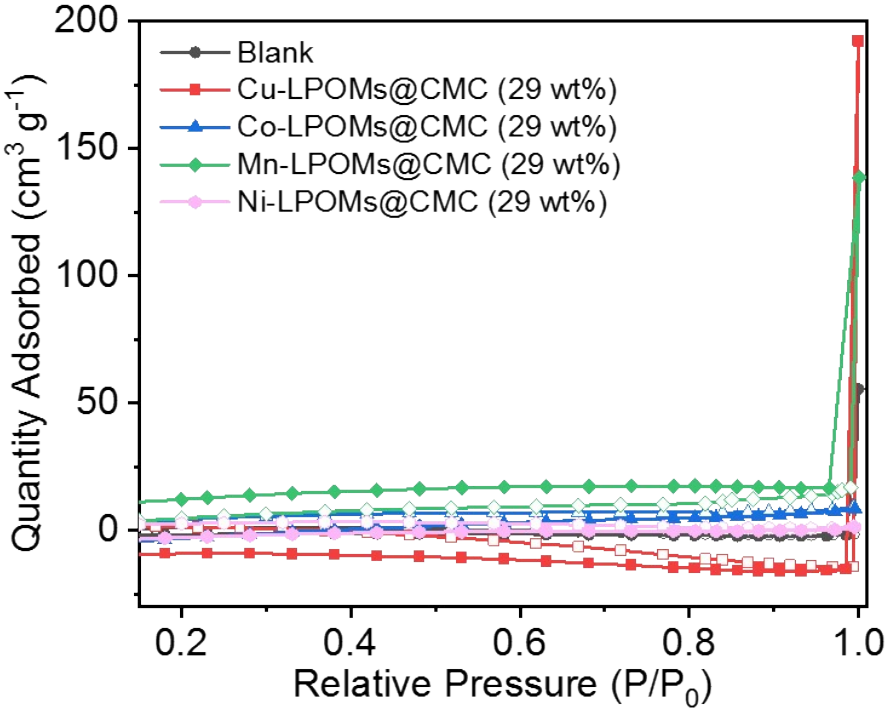

Figure S13. N_2 adsorption and desorption isotherms for CMC and TM-LPOMs@CMC (29 wt%) measured at 77 K.

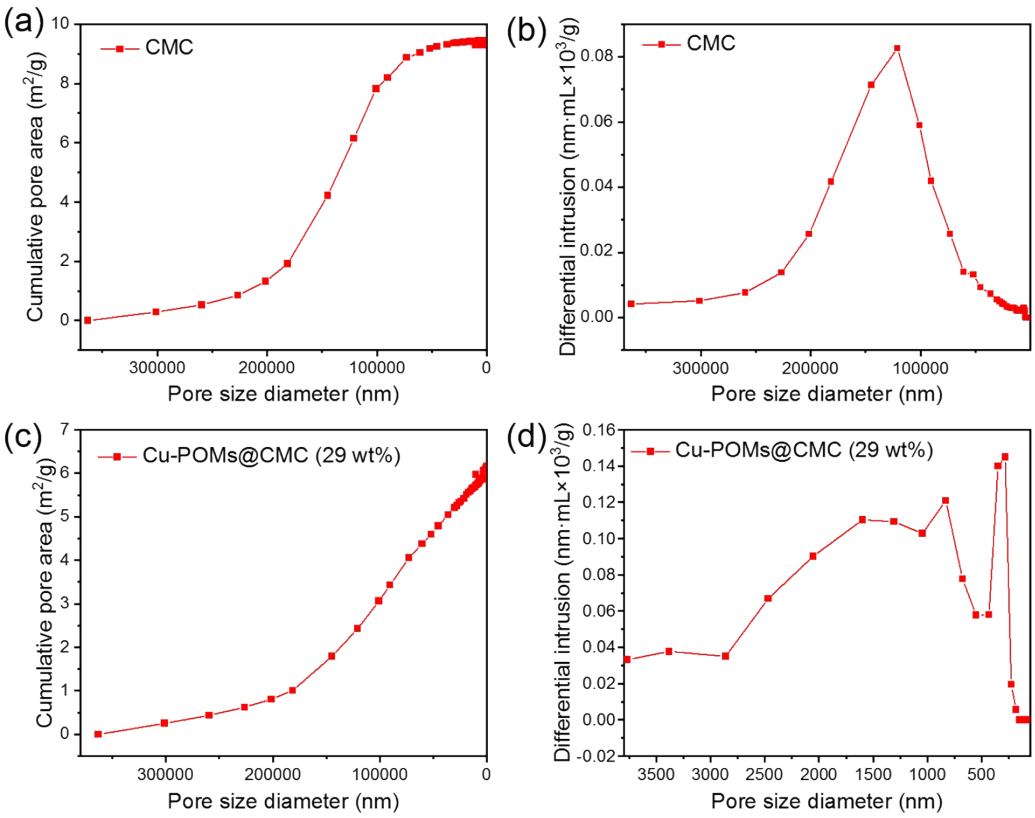

Figure S14. The Mercury intrusion porosimetry (MIP) curves of CMC and Cu-POMs@CMC (29 wt%). (a) Cumulative pore area vs pore size curves of CMC foam. (b) Differential intrusion vs pore size curves of CMC foam. (c) Cumulative pore area vs pore size curves of Cu-POMs@CMC (29 wt%) foam. (d) Differential intrusion vs pore size curves of Cu-POMs@CMC (29 wt%) foam.

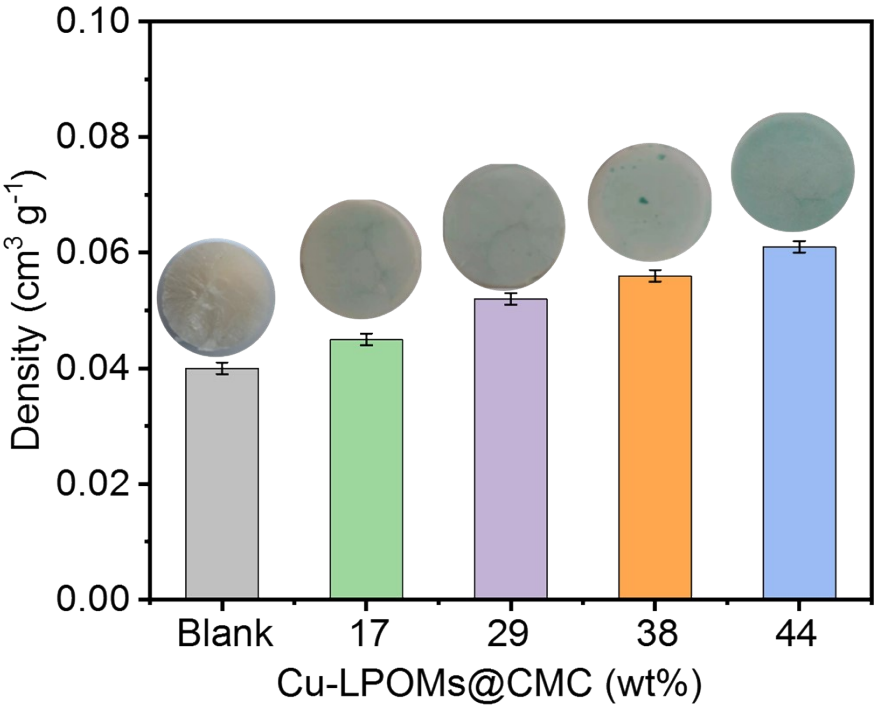

Figure S15. Photo images and densities of the Cu-LPOMs@CMC foams with various Cu-LPOMs loadings. The density test was conducted by Archimedes law and calculated the weight. All the experiments were conducted in triplicate.

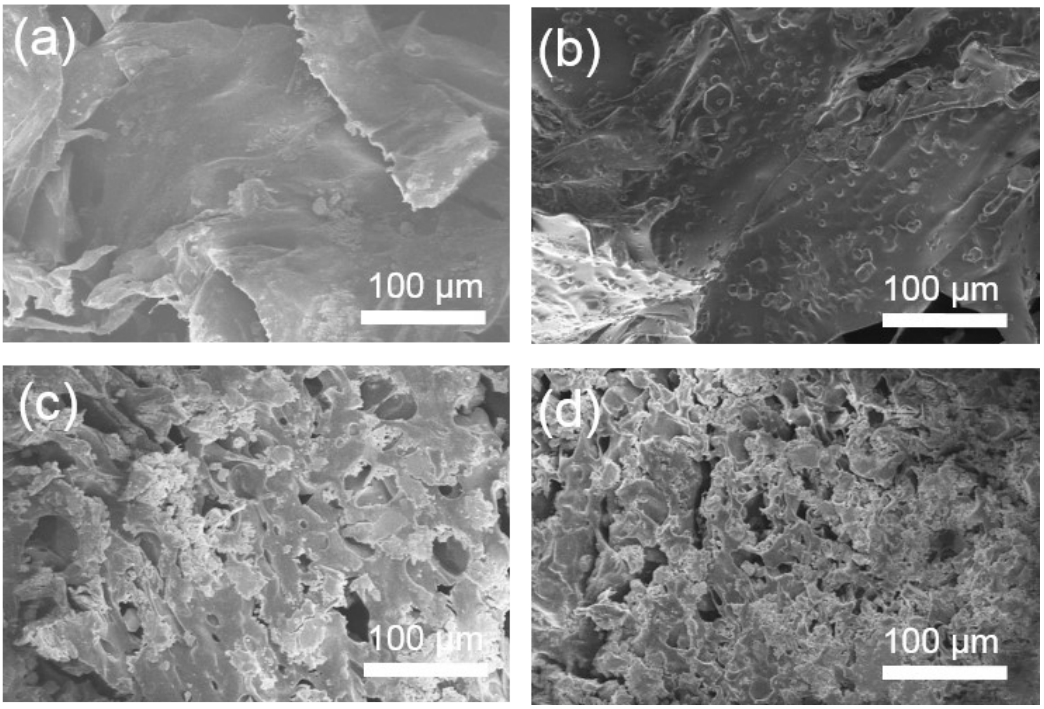

Figure S16. SEM images of the Cu-LPOMs@CMC foams with various Cu-LPOMs loadings. (a) Cu-LPOMs@CMC (17 wt%). (b) Cu-LPOMs@CMC (29 wt%). (c) Cu-LPOMs@CMC (38 wt%). (d) Cu-LPOMs@CMC (44 wt%).

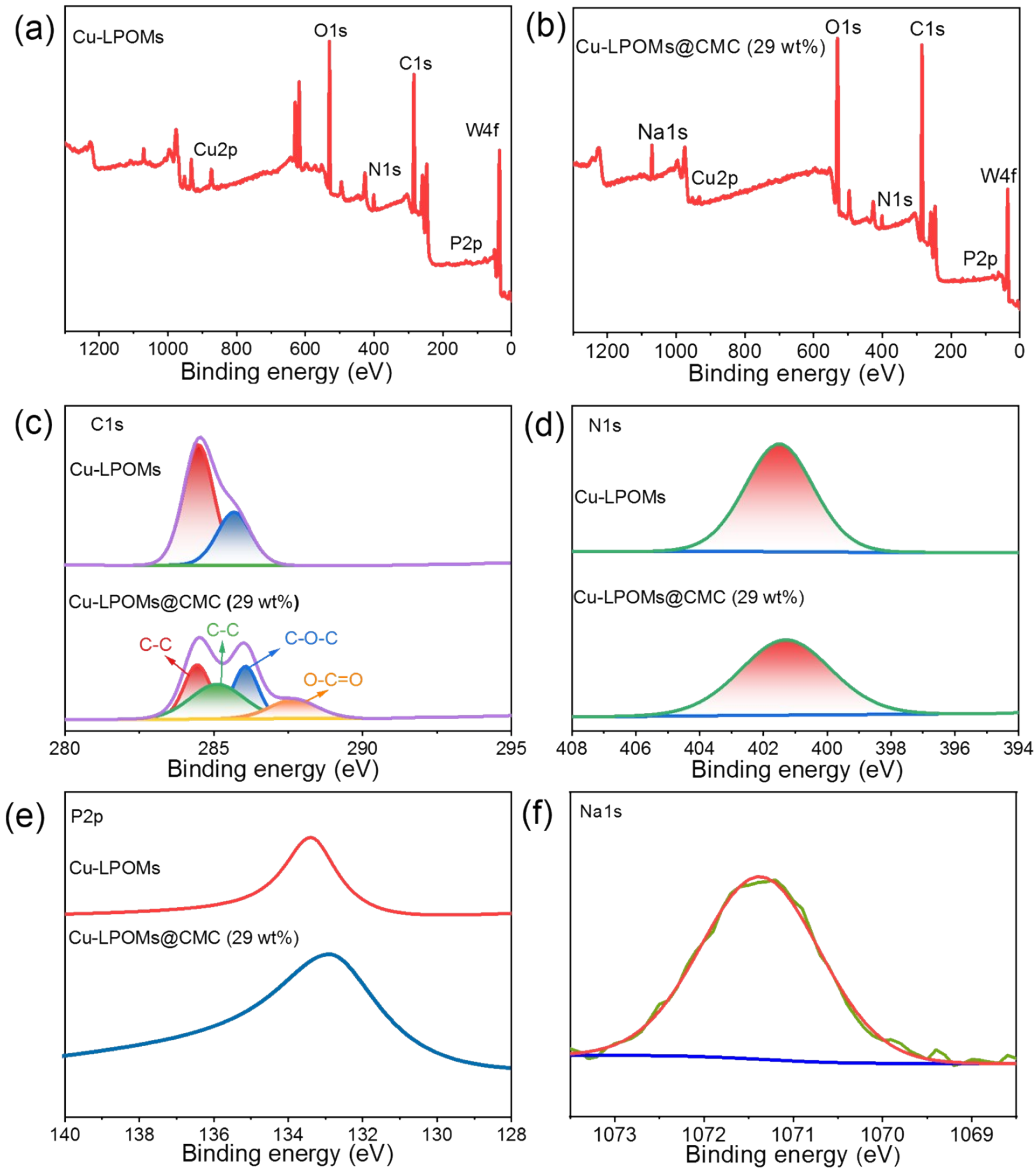

Figure S17. XPS spectrum of Cu-LPOMs and Cu-LPOMs@CMC (29 wt%). (a) Total XPS spectrum of Cu-LPOMs. (b) Total XPS spectrum of Cu-LPOMs@CMC (29 wt%). (c) XPS spectrum of C1s for Cu-LPOMs and Cu-LPOMs@CMC (29 wt%). (d) XPS spectrum of N1s for Cu-LPOMs and Cu-LPOMs@CMC (29 wt%). (e) XPS spectrum of P2p for Cu-LPOMs and Cu-LPOMs@CMC (29 wt%). (f) XPS spectrum of Na1s for Cu-LPOMs@CMC (29 wt%).

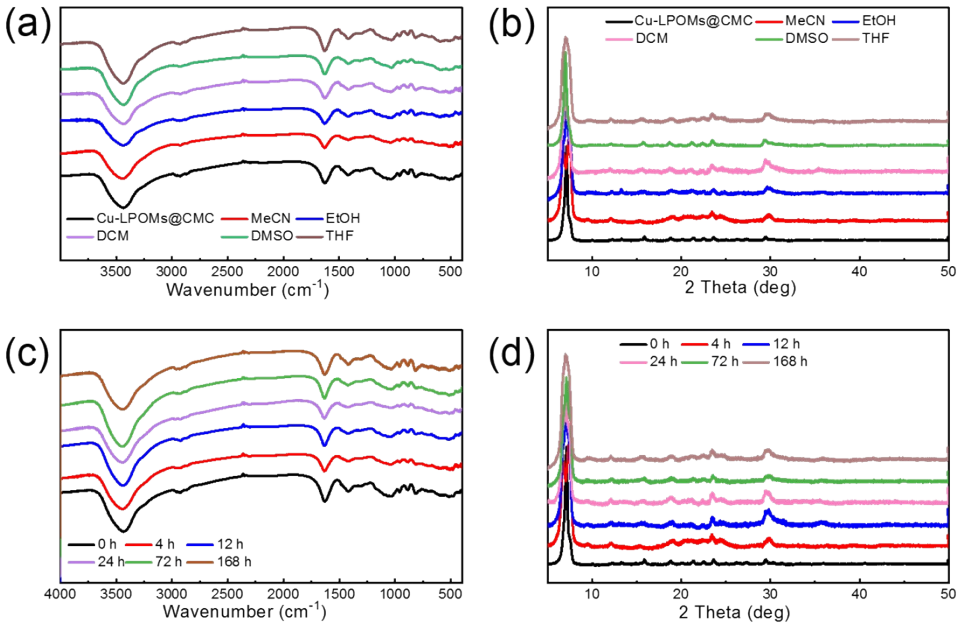

Figure S18. Stability test of Cu-LPOMs@CMC (29 wt%). (a) FT-IR spectra and (b) PXRD patterns of from leaching test of Cu-LPOMs@CMC (29 wt%) immersed in various solution. (c) FT-IR spectra and (d) PXRD patterns of Cu-LPOMs@CMC (29 wt%) immersed in the acetonitrile reaction solution for various time.

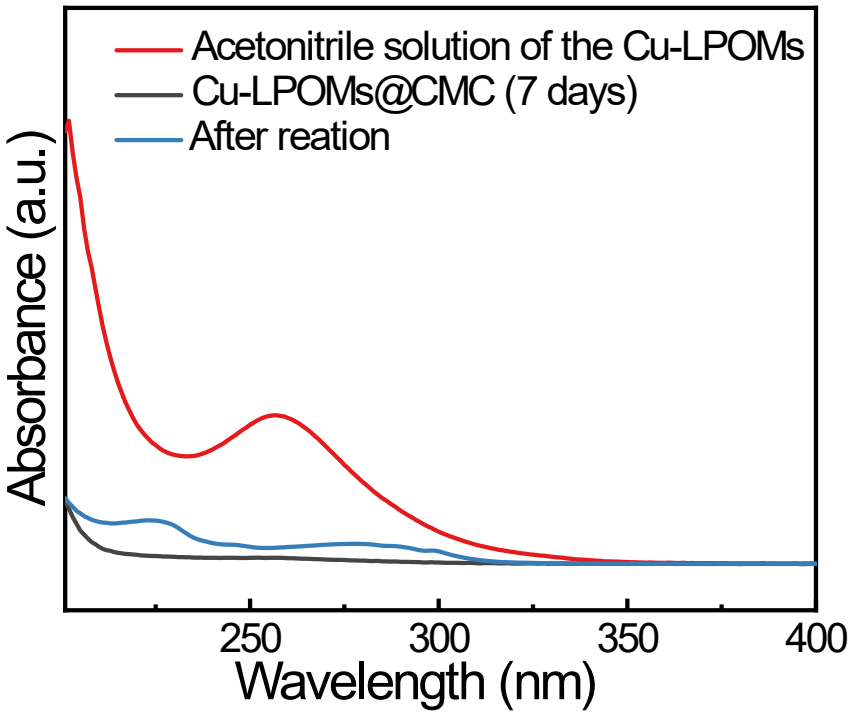

Figure S19. UV absorption spectra of the acetonitrile solution after immersing Cu-LPOMs@CMC (29 wt%) in it for 7 days and the Cu-LPOMs@CMC (29 wt%) after reaction.

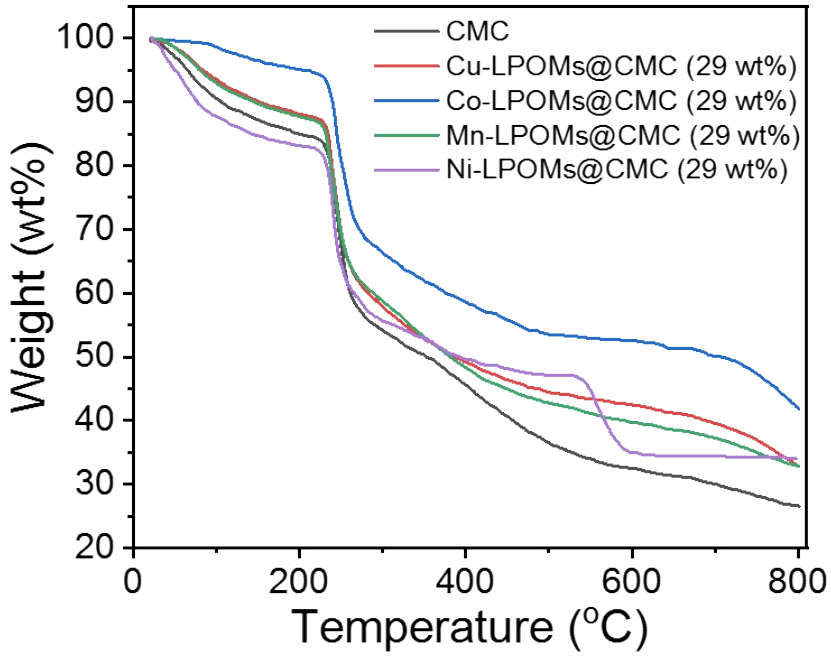

Figure S20. Thermogravimetric analysis (TGA) of CMC and TM-LPOMs@CMC (29 wt%).

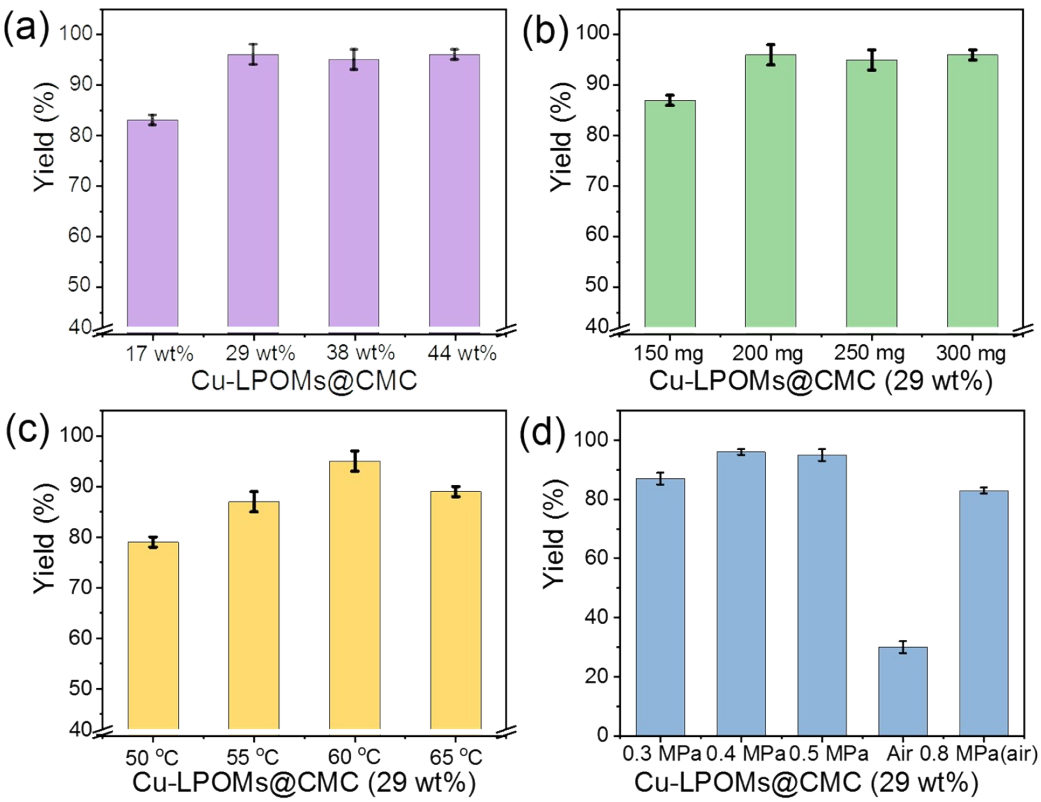

Figure S21. Optimization of the reaction conditions. (a) The effect of Cu-LPOMs@CMC foams with various Cu-LPOMs loadings on the model reaction. (b) The effect of Cu-LPOMs@CMC (29 wt%) mass on the model reaction. (c) The effect of different temperature on the model reaction. (d) The effect of different pressure on the model reaction.

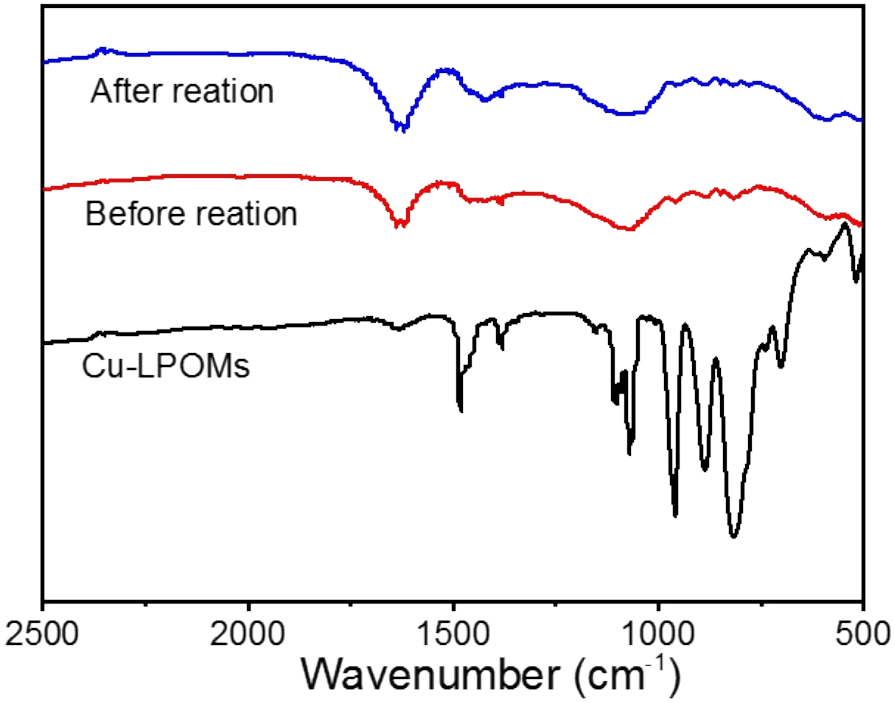

Figure S22. FT-IR spectra of Cu-LPOMs@CMC (29 wt%) before and after reactions.

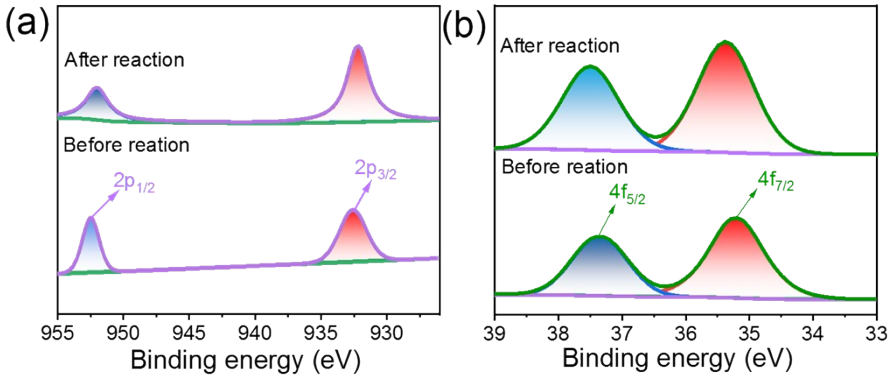

Figure S23. XPS spectra of Cu-LPOMs@CMC (29 wt%), (a) Cu2p and (b) W4f of before and after the reaction.

^{1}H NMR spectra of 2, 2'-dibenzothiazoledisulfde

^{1}H NMR (500 MHz, $CDCl_3$) δ: 7.87 (d, J = 8.2 Hz, 2H), 7.70 (d, J = 8.0 Hz, 2H), 7.39 (t, J = 8.3 Hz, 2H), 7.29 (t, J = 8.1 Hz, 2H).

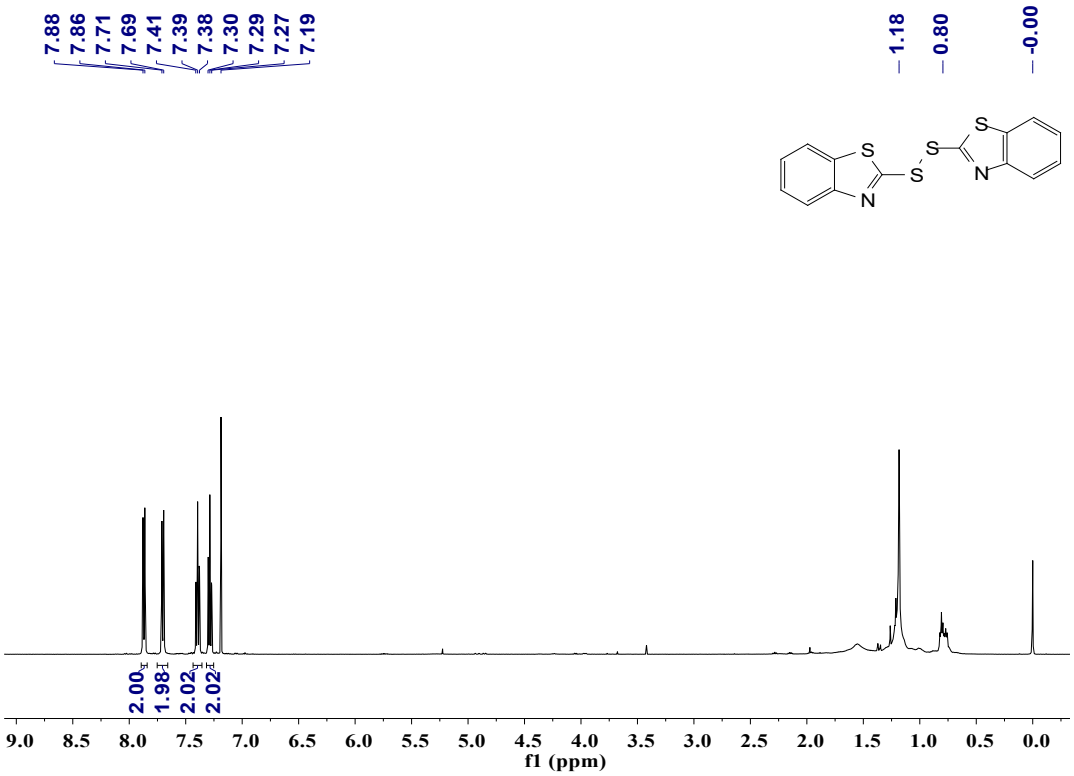

Figure S24. ^{1}H NMR spectra of intermediate 2, 2'-dibenzothiazoledisulfde.

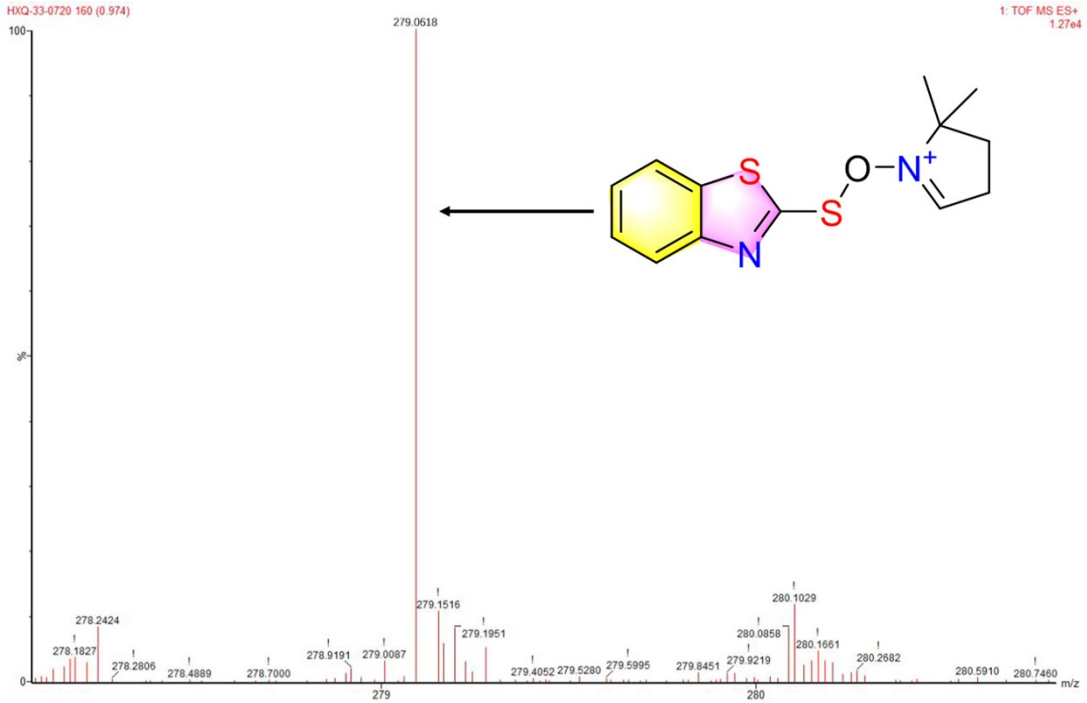

Figure S25. HRMS analysis of the adduct of thiol radical and DMPO.

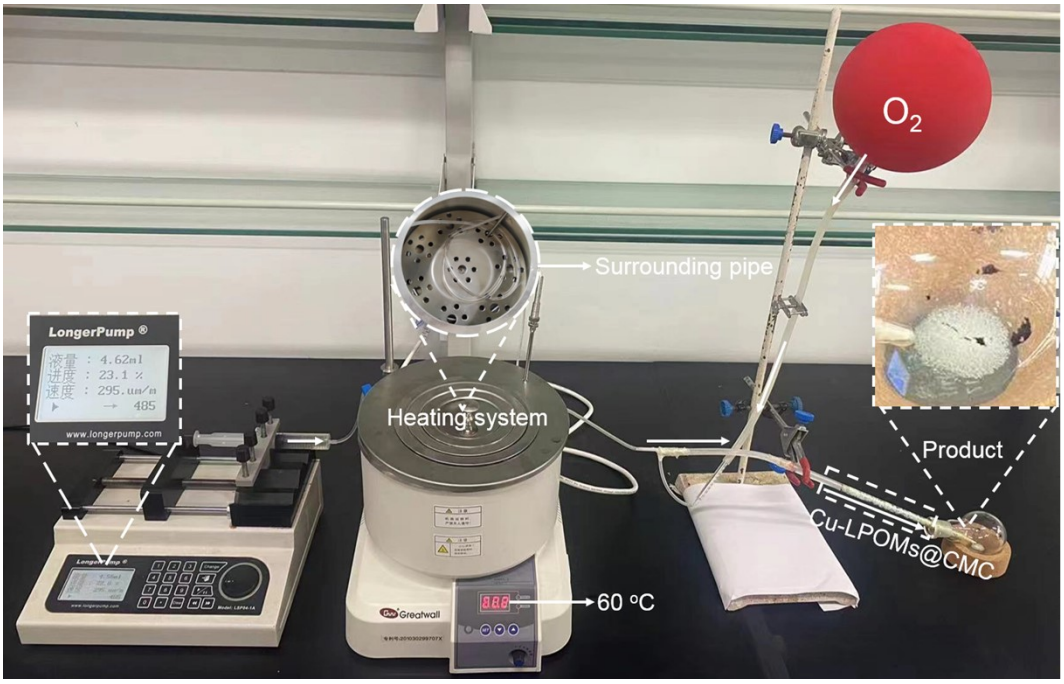

Figure S26. Schematic illustration of the flowing catalysis using the Cu-LPOM@CMC (29 wt%) as the catalyst (production rate, ~430 mg/h in a batch-experiment).

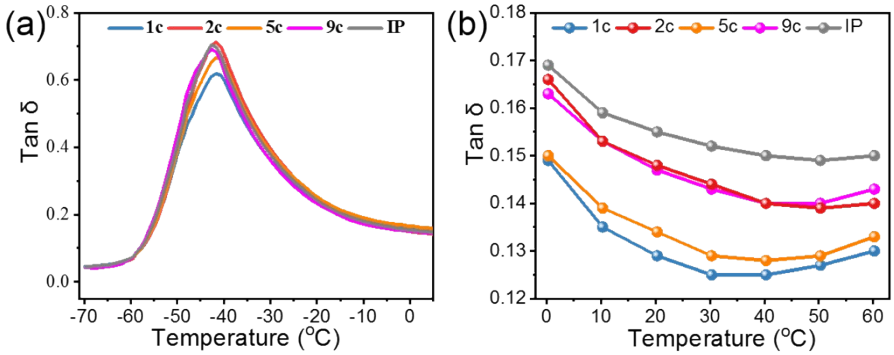

Figure S27. Dynamic mechanical analysis of sulfenamides rubber additives. (a) Dynamic mechanical analysis of fiver sulfenamides rubber additives. (b) Dynamic mechanical analysis from 0 to 60 °C.

Table S1. Optimization of reaction conditions.

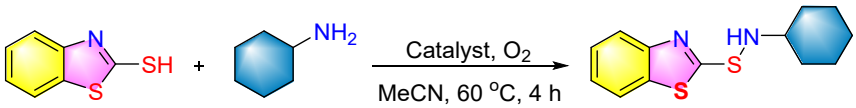

1a **1b** **1c**

Entry [a]	Catalysts	Yield (%) [c]
1	No	-
2	TBA_4-$H_3PW_{11}O_{39}$	-
3	$CuCl_2$	19
4	TBA_4-$HPW_{11}CuO_{39}$	82
5 [b]	TBA_4-$HPW_{11}CuO_{39}$	38
6	TBA_4-$HPW_{11}MnO_{39}$	-
7	TBA_4-$HPW_{11}NiO_{39}$	-
8	TBA_4-$HPW_{11}CoO_{39}$	-
9	CMC	-
10	Cu-LPOMs@CMC (17 wt%)	83
11	Cu-LPOMs@CMC (29 wt%)	96
12	Cu-LPOMs@CMC (38 wt%)	95
13	Cu-LPOMs@CMC (44 wt%)	96

[a] Reaction conditions: **1a** (1 mmol), **1b** (4 mmol), catalyst (200 mg), 60 °C, 0.4 MPa, 4 h, 10 mL MeCN. [b] Catalyst (80 mg). [c] Isolated yields.

Table S2. Analysis of test parameter data of sulfenamides rubber additives.

Test items	1c[a]	2c[a]	5c[a]	9c[a]	IP[b]
Mooney Viscosity (VM)	47.7	38.8	47.3	47.0	44.7
Scorch t5 time (min)	18.1	8.2	16.1	12.8	17.7
MH (dNm)	15.48	14.01	14.96	10.15	14.47
ML (dNm)	1.80	1.32	1.61	1.61	1.68
TS2 (sec)	283	126	269	158	274
Tc10 (sec)	252	108	235	89	250
Tc50 (sec)	374	203	368	254	348
Tc90 (sec)	662	484	647	582	593
Tc95 (sec)	816	608	769	696	706
Tc90-Tc10 (sec)	410	376	412	493	343
MH-ML (dNm)	13.68	12.69	13.35	8.54	12.79
Solidity (Shao A°)	75	73	77	71	76
Initial height (mm)	25.10	25.30	25.10	25.60	25.30
Deformation (mm)	3.0	4.0	3.9	4.2	4.5
Permanent deformation rate (%)	12.0	15.8	15.5	16.4	17.8
Internal temperature rise (°C)	41.6	50.4	55.2	47.3	57.8

[a] Laboratory preparation. [b] Industrial products (pre-dispersed master batch CBS-80).

Table S3. Oxidative synthesis of sulfonamide rubber additives by different catalyst.

Entry	Catalysts	Yeild	Ref.
1	Cu-LPOMs@CMC (29 wt%)	96	This work
2	TEMPO	88	1
3	$Co(phcy)(SO_3Na)_4$	90	2
4	NaOH, NaOCl	77	3
5	$Cu(CH_3COO)_2$	87	4
6	$NaClO/H_2O_2$	87	5

TEMPO: 2,2,6,6-tetramethylpiperidine-N-oxyl.

N-cyclohexyl-2-benzothiazolesulfenamide (1c).

White solid (96% yield), mp: 94-96 °C; ^{1}H NMR (500 MHz, $CDCl_3$) δ: 7.80 (dd, J = 11.7, 8.0 Hz, 2H), 7.39 (t, J = 7.6 Hz, 1H), 7.28 – 7.24 (m, 2H), 3.25 (d, J = 5.7 Hz, 1H), 2.93 – 2.87 (m, 1H), 2.09 (d, J = 10.7 Hz, 2H), 1.77 (dd, J = 13.1, 3.7 Hz, 2H), 1.62 (d, J = 13.1 Hz, 1H), 1.26 (q, J = 11.8 Hz, 5H); ^{13}C NMR (125 MHz, $CDCl_3$) δ: 135.0, 125.8, 123.5, 121.5, 121.0, 60.3, 33.7, 25.6, 24.9.

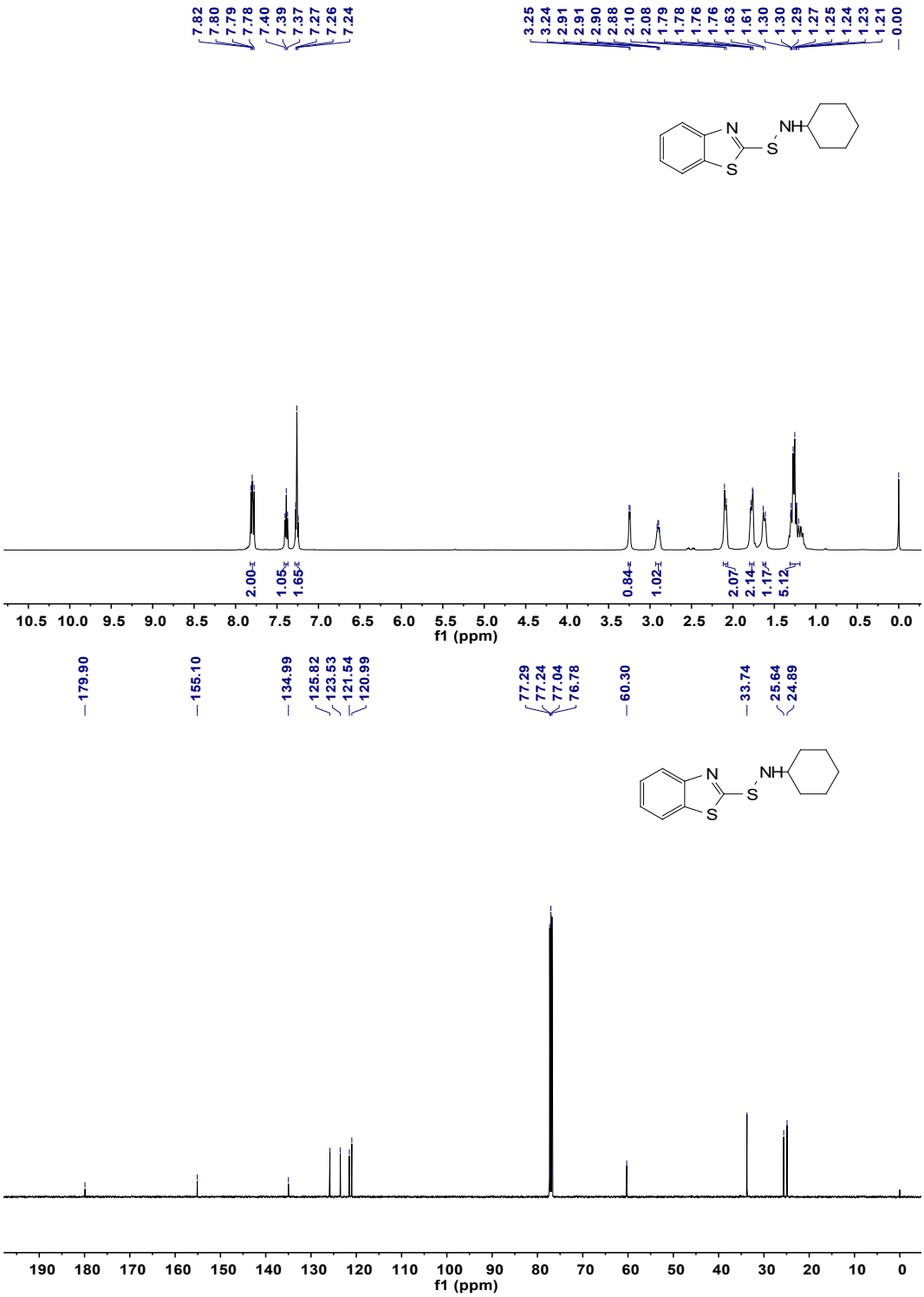

Figure S28. ^{1}H NMR and ^{13}C NMR spectra of compound **1c**.

N-(phenylmethyl)-2-Benzothiazolesulfenamide (2c)

White solid (63% yield), mp: 116-117 °C; ^{1}H NMR (500 MHz, $CDCl_3$) δ: 7.84 (dd, *J* = 13.0, 8.0 Hz, 2H), 7.44 – 7.37 (m, 5H), 7.33 – 7.28 (m, 2H), 4.29 (d, *J* = 5.9 Hz, 2H), 3.55 (s, 1H); ^{13}C NMR (125 MHz, $CDCl_3$) δ: 138.5, 128.7, 128.5, 128.0, 126.0, 123.8, 121.7, 121.1, 57.1.

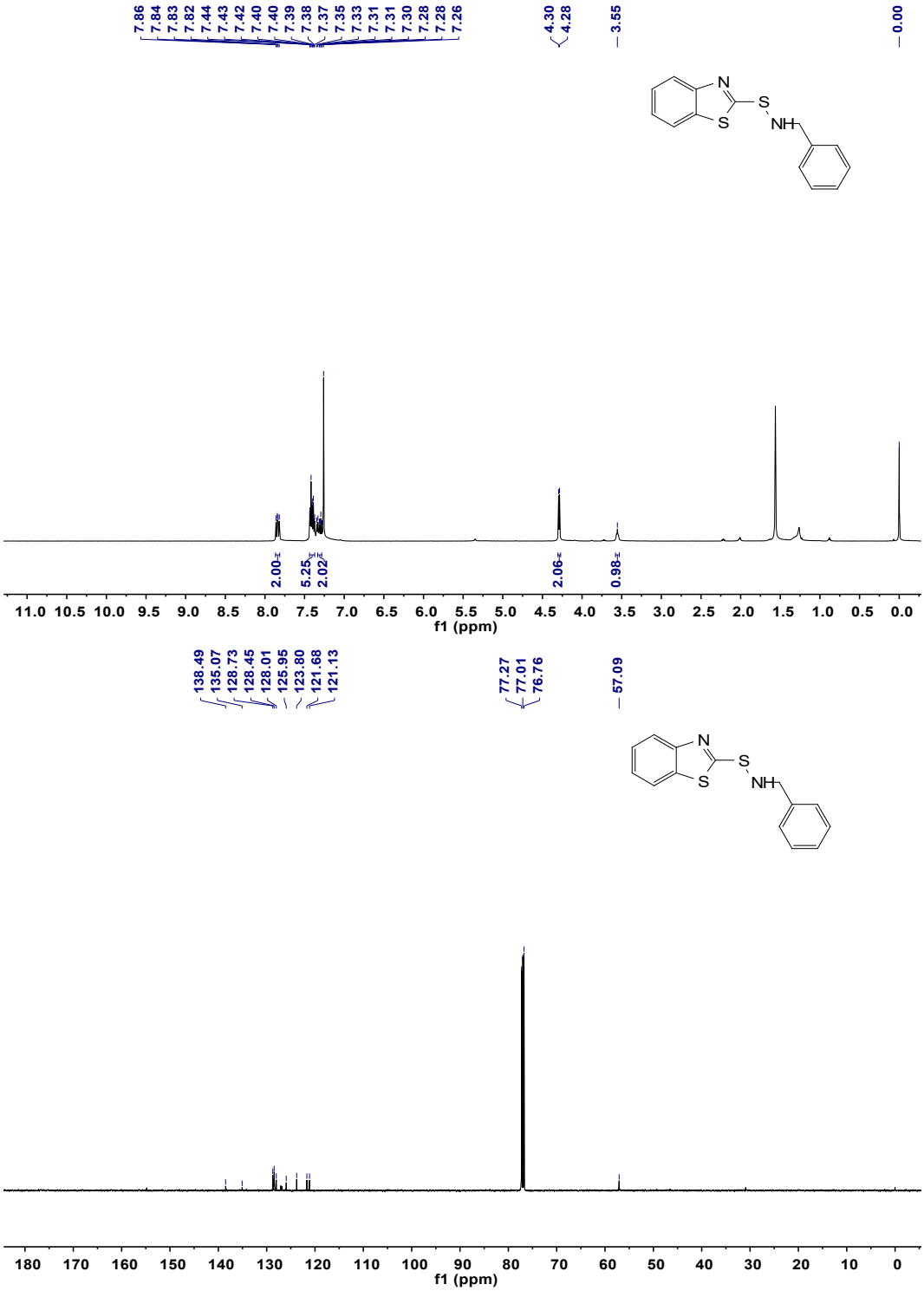

Figure S29. ^{1}H NMR and ^{13}C NMR spectra of compound **2c**.

N-[(4-chlorophenyl)methyl]-2-benzothiazolesulfenamide (3c).

^{1}H NMR (500 MHz, $CDCl_3$) δ: 7.84 (dd, J = 15.7, 8.0 Hz, 2H), 7.42 (td, J = 7.8, 7.3, 1.2 Hz, 1H), 7.35 (s, 4H), 7.32 – 7.28 (m, 1H), 4.26 (d, J = 5.8 Hz, 2H), 3.59 (t, J = 5.9 Hz, 1H); ^{13}C NMR (125 MHz, $CDCl_3$) δ: 154.7, 136.9, 135.0, 133.9, 129.9, 128.9, 126.0, 123.9, 121.7, 121.2, 56.2.

Figure S30. ^{1}H NMR and ^{13}C NMR spectra for compound **3c**.

N-[(4-bromophenyl)methyl]-2-Benzothiazolesulfenamide (4c)

White solid (58% yield), mp: 116-120 °C; ^{1}H NMR (500 MHz, $CDCl_3$) δ: 7.84 (dd, *J* = 15.7, 8.0 Hz, 2H), 7.51 (d, *J* = 8.0 Hz, 2H), 7.43 (d, *J* = 7.5 Hz, 1H), 7.30 (t, *J* = 7.6 Hz, 3H), 4.24 (d, *J* = 5.8 Hz, 2H), 3.59 (t, *J* = 5.9 Hz, 1H); ^{13}C NMR (125 MHz, $CDCl_3$) δ: 131.8, 130.2, 126.0, 123.9, 121.7, 121.2, 76.8, 56.2.

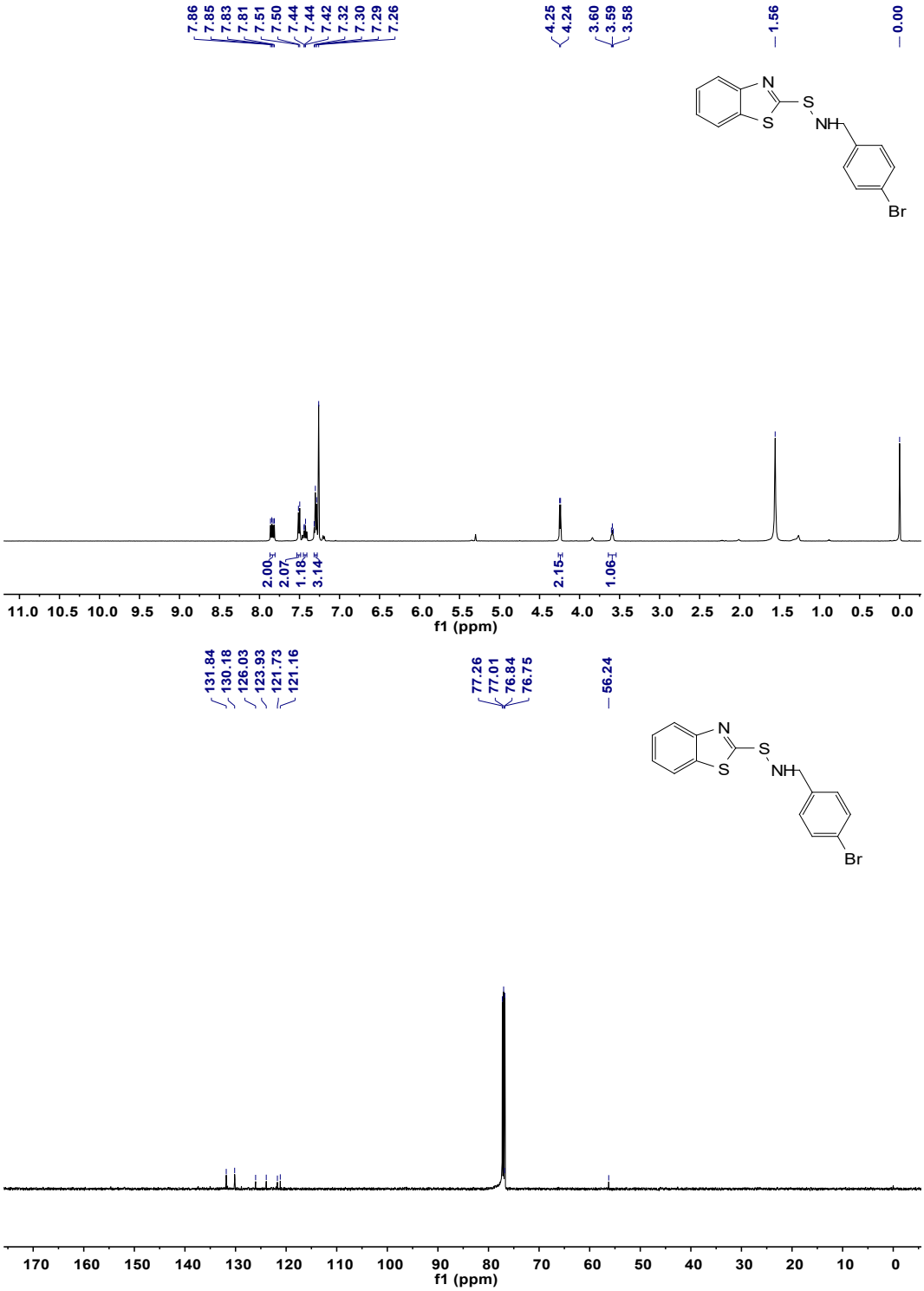

Figure S31. ^{1}H NMR and ^{13}C NMR spectra of compound **4c**.

N-[(4-methylphenyl)methyl]-2-Benzothiazolesulfenamide (5c)

White solid (70% yield), mp: 120-123 °C; ^{1}H NMR (500 MHz, $CDCl_3$) δ: 7.83 (dd, *J* = 12.6, 8.0 Hz, 2H), 7.44 – 7.38 (m, 1H), 7.32 – 7.27 (m, 3H), 7.19 (d, *J* = 7.8 Hz, 2H), 4.24 (d, *J* = 5.9 Hz, 2H), 3.51 (t, *J* = 5.7 Hz, 1H), 2.36 (s, 3H); ^{13}C NMR (125 MHz, $CDCl_3$) δ: 154.9, 137.8, 135.5, 129.4, 128.4, 125.9, 123.8, 121.7, 121.1, 56.8, 21.2.

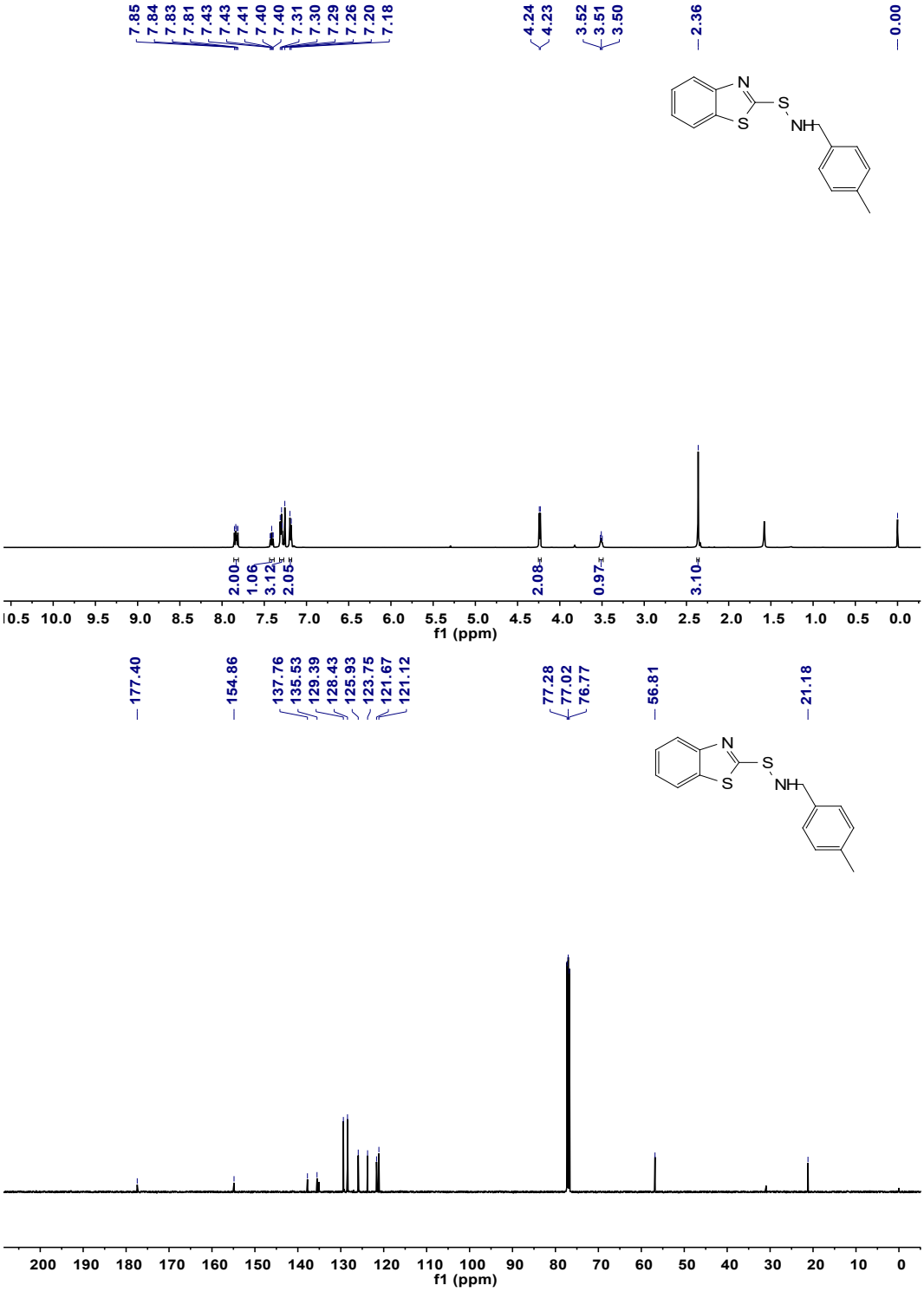

Figure S32. ^{1}H NMR and ^{13}C NMR spectra of compound **5c**.

N-tert-Butyl-2-benzothiazolesulfenamide (6c)

White solid (87% yield), mp: 105-106 °C; ^{1}H NMR (500 MHz, $CDCl_3$) δ: 7.78 (dd, *J* = 10.9, 8.0 Hz, 2H), 7.40 – 7.36 (m, 1H), 7.25 (d, *J* = 12.3 Hz, 1H), 3.42 (s, 1H), 1.28 (s, 9H); ^{13}C NMR (125 MHz, $CDCl_3$) δ: 155.1, 134.9, 125.8, 123.5, 121.5, 120.9, 55.6, 29.0.

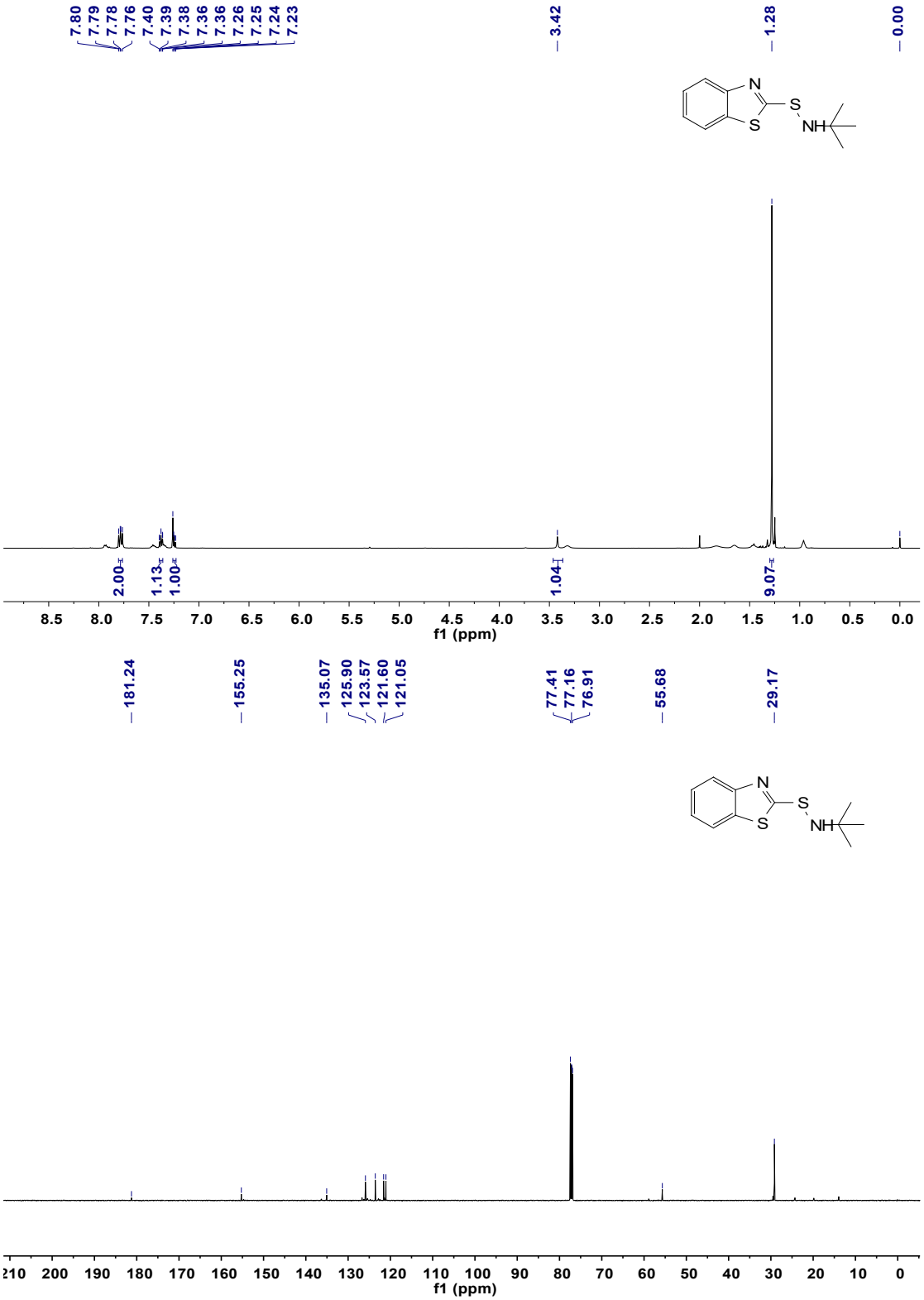

Figure S33. ^{1}H NMR and ^{13}C NMR spectra of compound **6c**.

N- butyl-2-benzothiazolesulfenamide (7c)

Colorless oil (96% yield); ^{1}H NMR (500 MHz, $CDCl_3$) δ: 7.70 (d, J = 8.2 Hz, 1H), 7.63 (d, J = 8.0 Hz, 1H), 7.26 – 7.21 (m, 1H), 7.13 – 7.07 (m, 1H), 3.30 (d, J = 6.0 Hz, 1H), 2.98 – 2.91 (m, 2H), 1.47 – 1.39 (m, 2H), 1.27 – 1.19 (m, 2H), 0.78 (ddd, J = 9.1, 6.7, 1.8 Hz, 3H); ^{13}C NMR (125 MHz, $CDCl_3$) δ: 155.0, 135.0, 125.9, 123.6, 121.5, 121.1, 52.8, 32.7, 20.0, 14.0.

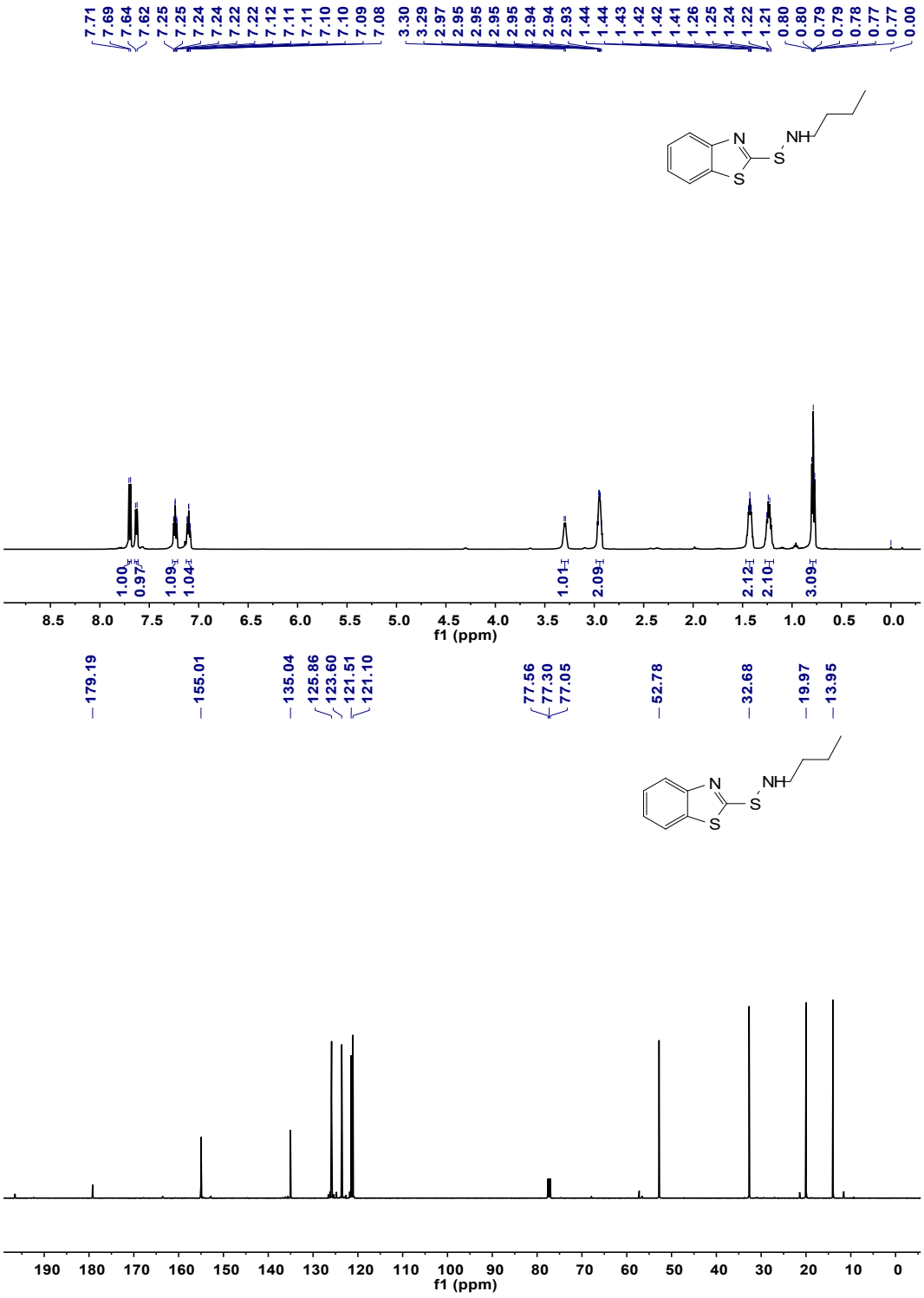

Figure S34. ^{1}H NMR and ^{13}C NMR spectra of compound **7c**.

N-(cyclohexylmethyl)-2-benzothiazolesulfenamide (8c).

^{1}H NMR (500 MHz, $CDCl_3$) δ: 7.81 (t, J = 9.0, 2H), 7.43 – 7.37 (m, 1H), 7.28 (s, 1H), 3.26 (s, 1H), 2.99 (s, 2H), 1.89 – 1.67 (m, 5H), 1.56 (tt, J = 6.8, Hz, 1H), 1.32 – 1.17 (m, 3H), 0.98 (d, J = 15.0 Hz, 2H); ^{13}C NMR (126 MHz, $CDCl_3$) δ: 178.9, 155.0, 135.0, 125.9, 123.6, 121.6, 121.1, 60.0, 38.8, 30.9, 26.5, 25.9.

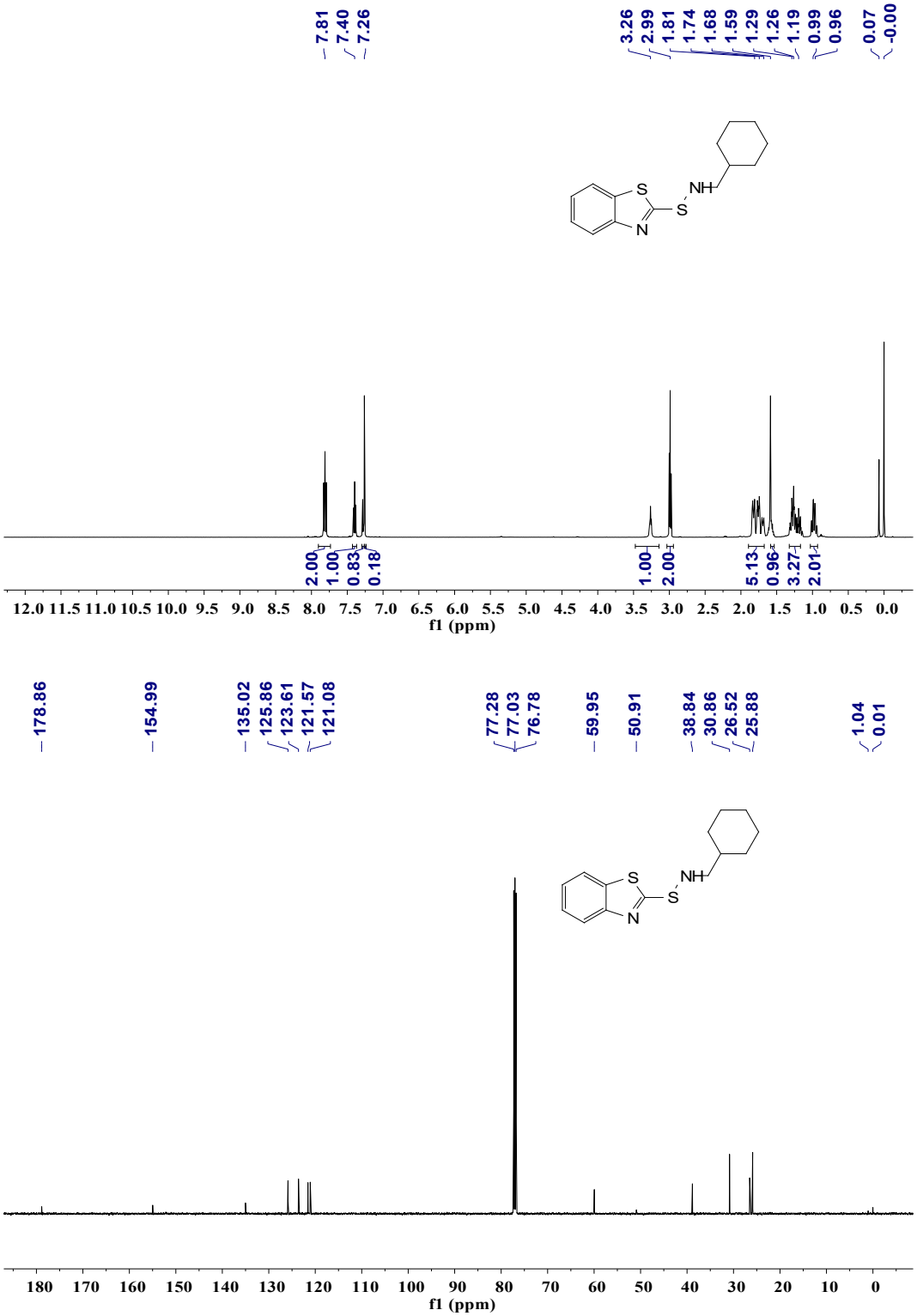

Figure S35. ^{1}H NMR and ^{13}C NMR spectra for compound **8c**.

N,N-diethyl-2-Benzothiazolesulfenamide (9c)

Light yellow oil (73% yield); ^{1}H NMR (500 MHz, $CDCl_3$) δ: 7.71 (d, J = 8.1 Hz, 1H), 7.66 (d, J = 7.9 Hz, 1H), 7.29 – 7.25 (m, 1H), 7.16 – 7.11 (m, 1H), 3.05 (q, J = 7.1 Hz, 4H), 1.14 (t, J = 7.1 Hz, 6H); ^{13}C NMR (125 MHz, $CDCl_3$) δ: 155.2, 135.0, 125.8, 123.5, 121.5, 120.9, 52.5, 31.0, 13.5.

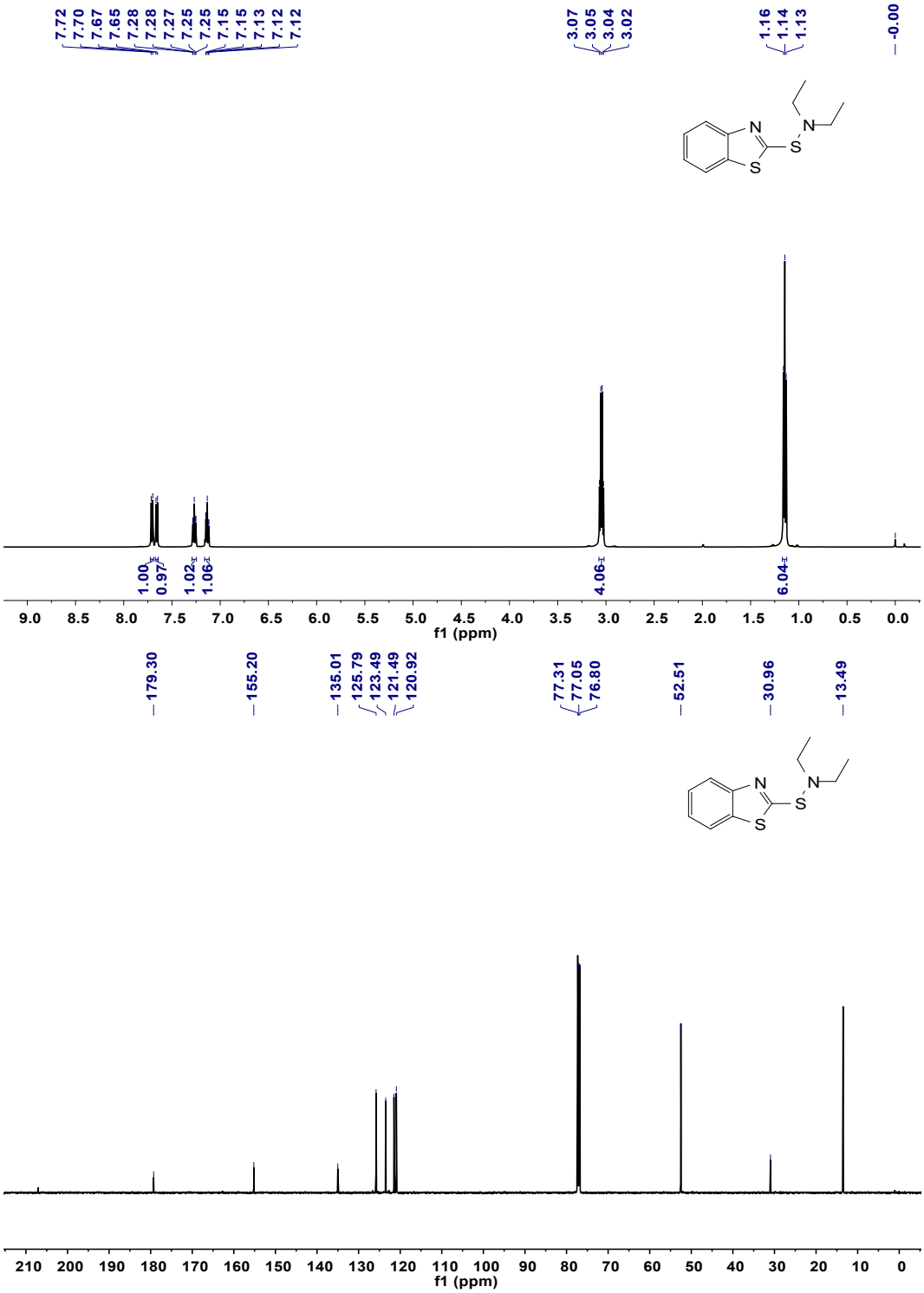

Figure S36. ^{1}H NMR and ^{13}C NMR spectra of compound **9c**.

2-[(1-piperidinylthio]-Benzothiazole (11c)

Colorless oil (84% yield); ^{1}H NMR (500 MHz, $CDCl_3$) δ: 7.81 (dd, J = 13.0, 8.0 Hz, 2H), 7.39 (t, J = 7.7 Hz, 1H), 7.28 – 7.24 (m, 1H), 3.23 (t, J = 5.4 Hz, 4H), 1.74 (t, J = 5.7 Hz, 4H), 1.53 (d, J = 5.8 Hz, 2H); ^{13}C NMR (125 MHz, $CDCl_3$) δ: 135.2, 125.8, 123.6, 121.7, 121.0, 58.1, 27.38, 23.1.

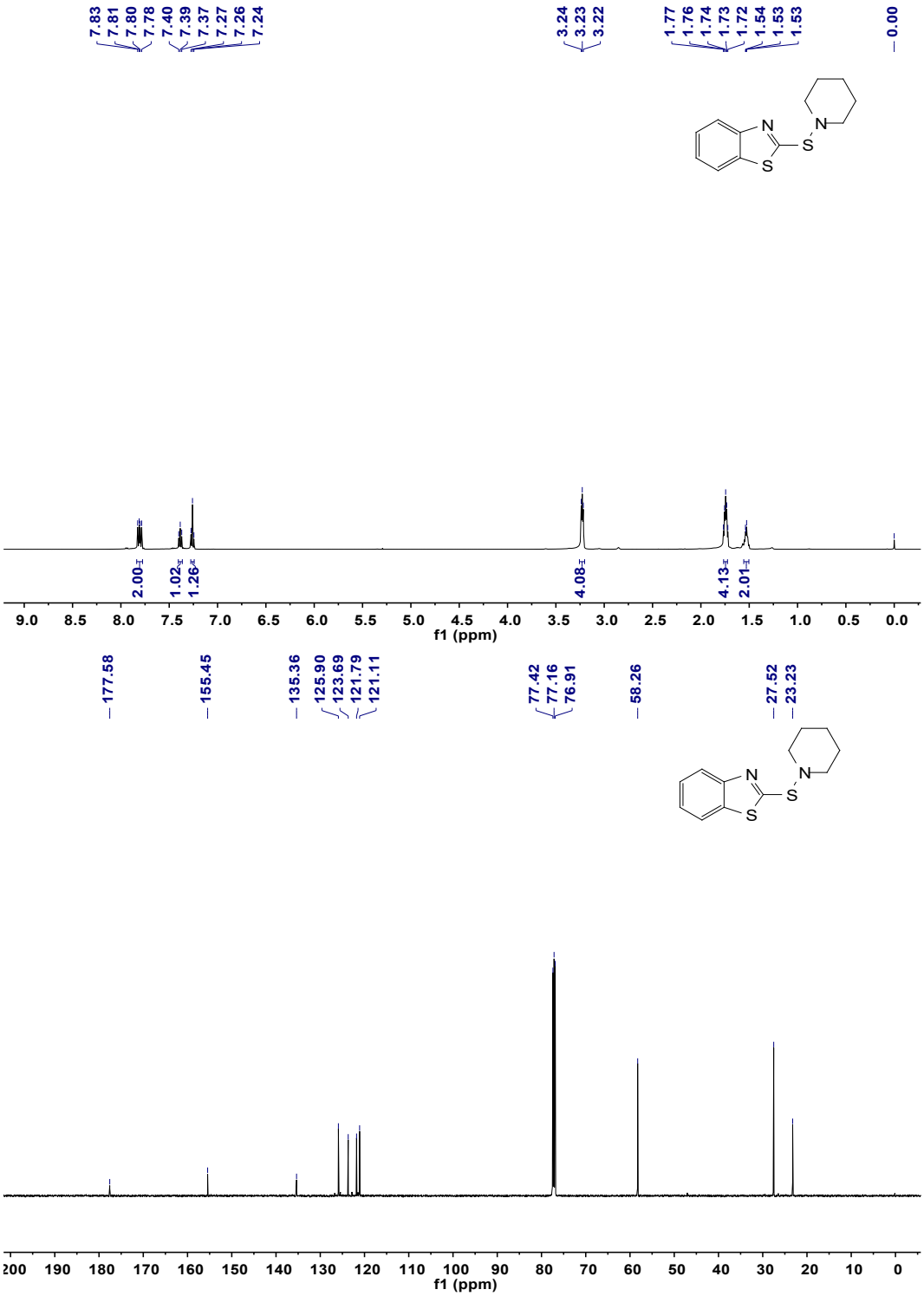

Figure S37. ^{1}H NMR and ^{13}C NMR spectra of compound **11c**.

2-(4-morpholinylthio)-Benzothiazole (12c)

White solid (81% yield), mp: 80-82 °C; ^{1}H NMR (500 MHz, $CDCl_3$) δ: 7.85 (d, J = 8.1 Hz, 1H), 7.81 (d, J = 7.9 Hz, 1H), 7.44 – 7.39 (m, 1H), 7.31 – 7.27 (m, 1H), 3.85 – 3.81 (m, 4H), 3.32 – 3.27 (m, 4H); ^{13}C NMR (125 MHz, $CDCl_3$) δ: 175.0, 155.1, 135.0, 126.0, 124.0, 121.9, 121.1, 67.9, 56.6.

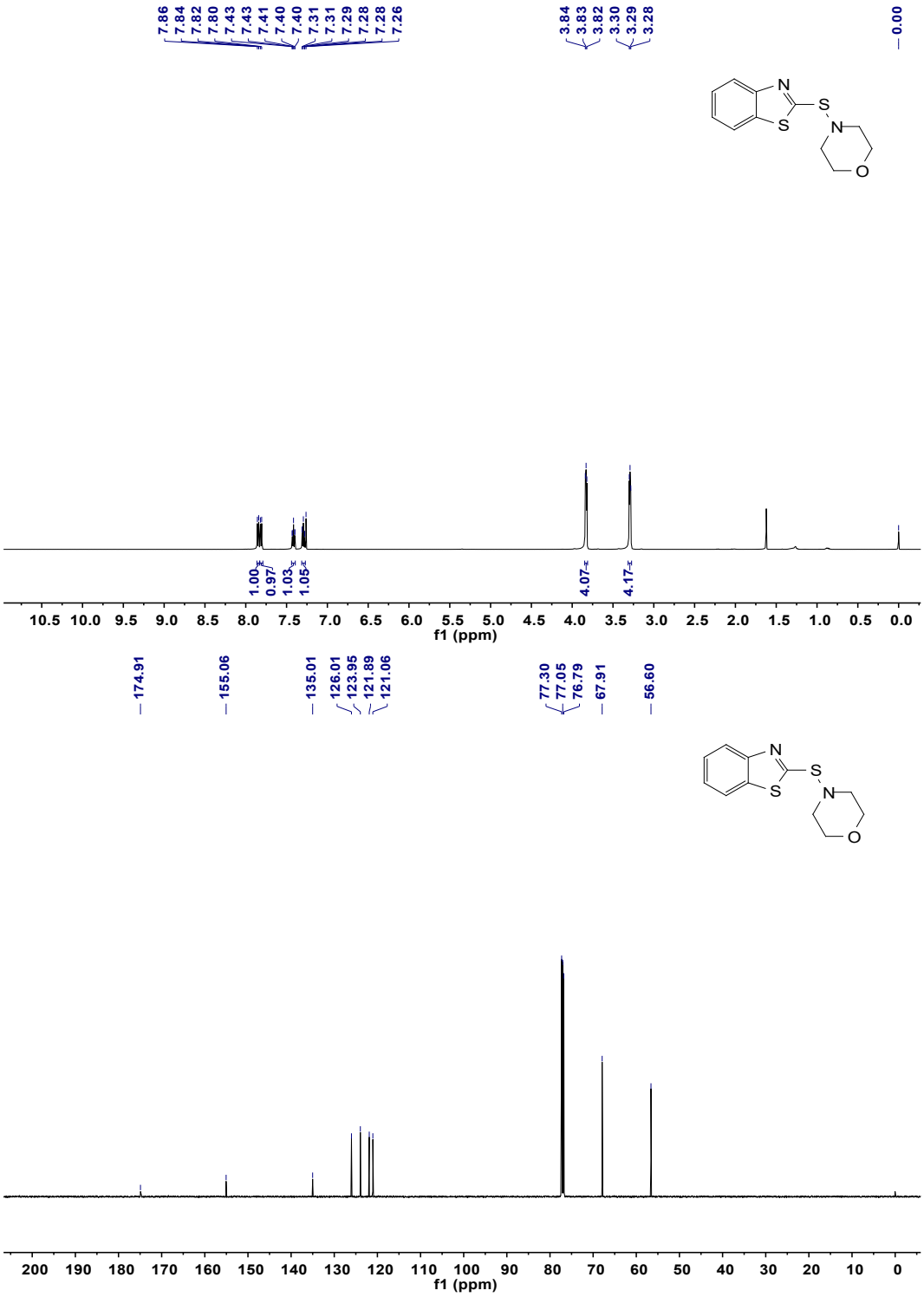

Figure S38. ^{1}H NMR and ^{13}C NMR spectra of compound **12c**.

References

[1] L. Yang, S. Li, Y. Dou, S. Zhen, H. Li, P. Zhang, B. Yuan, G. Yang, *Asian J. Org. Chem*., 2017, **6**, 265-268.

[2] Y. Dou, X. Huang, H. Wang, L. Yang, H. Li, B. Yuan, G. Yang, *Green Chem*., 2017, **19**, 2491-2495.

[3] D. J. Banks, P. Wiseman, *J. Appl. Chem*., 1968, **18**, 262-265.

[4] H. Li, F. Han, L. Jiang, T. Yang, L. Du, J. Zhu, *Ind. Eng. Chem. Res*., 2021, **60**, 14134-14142.

[5] B. Zhong, H. Dong, J. Lin, Z. Jia, Y. Luo, D. Jia, F. Liu, *Ind. Eng. Chem. Res*., 2017, **56**, 9135-9142.